Dynamic regulation of mRNA acetylation at synapses by spatial memory in mouse hippocampus

Hai-Qian Zhou[1,2#], Zhen Zhu[1#], Jia-Wei Zhang[1#], Wei-Peng Lin[1,3,4], Hao-JY Jin[1], Yang-Yang Ding[1], Shuai Liu[1,3*] and Dong-Min Yin[1,3,5*]

[1]Key Laboratory of Brain Functional Genomics, Ministry of Education and Shanghai, Affiliated Mental Health Center, School of Life Science, East China Normal University, Shanghai, 200062, China

[2]Department of Neurology, Shanghai Fifth People's Hospital, Fudan University, Shanghai, 200240, China.

[3]Shanghai Changning Mental Health Center, Affiliated Mental Health Center of East China Normal University, Shanghai, 200335, China

[4]Chongqing Key Laboratory of Precision Optics, Chongqing Institute of East China Normal University, Chongqing, 401120, China

[5]NYU-ECNU Institute of Brain and Cognitive Science at NYU Shanghai, Shanghai, 200062, China

[#]H-Q Z, Z Z and J-W Z contributed equally to this work.

[*]Correspondence should be addressed to

Prof. Shuai Liu,

Email: sliu@psy.ecnu.edu.cn

or

Prof. Dong-Min Yin,

Email: dmyin@brain.ecnu.edu.cn

Abstract

Precise regulation of protein synthesis is critical to a variety of brain functions including long-term memory. Dysregulated protein synthesis has been implicated in several disorders characterized by memory deficits. In contrast to mRNA methylation such as N6-methyladenosine (m6A) that was widely studied in memory, the regulation and function of mRNA acetylation in memory remain largely unknown. N4-acetylcytidine (ac4C), the only known form of RNA acetylation in eukaryotes, has recently been shown to regulate mRNA stability and translation efficiency. In this study, we identified the ac4C epitranscriptome through ac4C-RNA immunoprecipitation followed by next-generation sequencing (acRIP-seq) in the homogenates and synaptosomes of mouse hippocampus, a brain region critical for spatial memory. The task of Morris water maze (MWM) was employed to induce and evaluate memory acquisition and forgetting processes. Interestingly, the levels of ac4C mRNA were upregulated in the synaptosomes after memory formation but returned to normal levels after memories were naturally forgotten. The dynamic changes of ac4C-mRNAs regulated by memory were validated by ac4C dot-blot, Liquid Chromatography-Tandem Mass Spectrometry (LC-MS/MS), and acRIP-qPCR analysis. We further demonstrate that NAT10, the ac4C writer, in mouse hippocampus is important for spatial memory via regulating memory-related mRNAs, proteins, and ultimately synaptic plasticity. Lastly, we generated a freely-accessible website (http://ac4catlas.com) that included the dataset of ac4C epitranscriptome in mouse hippocampus. Altogether these results reveal a previously unappreciated mechanism underlying memory.

Introduction

Precise regulation of protein synthesis at the right place and right time is important for various brain functions including learning and memory[1,2]. For instance, local protein synthesis near stimulated synapses plays critical roles in synaptic plasticity and memory consolidation[3,4]. Mechanistically, epigenetic regulations on DNA and histone proteins have been widely studied in the context of learning and memory[5,6]. However, the roles of chemical modifications on mRNA in learning and memory have only become appreciated in recent years[7-9]. Especially, N6-methyladenosine (m6A), a well-studied form of mRNA methylation has been shown to regulate synaptic plasticity as well as learning and memory[10-12].

N4-acetylcytidine (ac4C) is the only known form of RNA acetylation in eukaryotes[13]. Initially, ac4C was identified in the transfer RNA (tRNA) anticodon[14-17]. Later studies revealed that ac4C also occurred in the 18S ribosomal RNA (rRNA)[18]. More recently, ac4C has been found in mRNA from mammalian cells, where it was reported to promote mRNA stability and translational efficiency[19,20]. N-acetyltransferase 10 (NAT 10) is the only known ac4C writer in mammalian cells[21]. NAT10-mediated mRNA acetylation has been reported to regulate tumorigenesis[22,23], stem cell differentiation[24], cardiac remodeling[25], germ cell maturation[26] and pain signaling in the spinal cord[27,28]. However, the function and regulatory mechanisms of mRNA acetylation in the brain remain poorly understood.

The hippocampus plays an important role in learning and memory[29]. Pyramidal neurons in the CA3 region of hippocampus establish direct projection to CA1 pyramidal neurons through the Schaffer collateral (SC) pathway, known as the SC-CA1 synapse. The glutamatergic transmission at SC-CA1 synapses was found to be enhanced following training in the Morris water maze (MWM)[30], a behavioral paradigm for learning and memory[31]. Long-term potentiation (LTP), a widely-studied form of synaptic plasticity in hippocampus, is most closely linked to learning and memory[32]. Several studies showed that mRNAs and ribosomes were present in the synaptosomes, contributing to protein synthesis at synapses[33]. In principle, neural activities can

regulate local protein synthesis through post-transcriptional modification of synaptic mRNAs[34]. However, whether synaptic mRNAs were subjected to NAT10-mediated acetylation and whether this process contributed to synaptic plasticity and memory remain elusive.

In this study, we conducted ac4C dot-blots, liquid chromatography-tandem mass spectrometry (LC-MS/MS) and acRIP-seq to study the ac4C modification of mRNA in mouse hippocampus during and after training in the MWM. We found that ac4C modification of mRNA was increased in the synaptosomes (SYN), rather than in the homogenates (HOM), following memory, and subsequently returned to baseline after memory forgetting. We further demonstrate that NAT10, the ac4C writer, in mouse hippocampus is important for memory through regulating memory-related mRNAs, proteins and ultimately synaptic plasticity. Collectively these results demonstrate the importance of mRNA acetylation in memory. The dataset of ac4C epitranscriptome from mouse hippocampus is freely accessible at the website (http://ac4catlas.com/).

Results

Presence of ac4C modification of polyA RNA in mouse hippocampus

Recent studies raised the debate about the presence of ac4C mRNA from mammalian cells[35,36]. We first investigate whether ac4C is a detectable modification of mRNA from mouse hippocampus. To this end, we purified polyadenylated (polyA) RNA from HOM of mouse hippocampus and determine their ac4C levels using LC-MS/MS. The purity of polyA RNA was verified by bioanalyzer analysis (Figure 1A and 1B) and dramatic reduction of 18S rRNA relative to total RNA in the analysis of reverse transcription followed by quantitative PCR (RT-qPCR) (Figure 1C). An ac4C standard curve was generated to calculate the stoichiometry levels of ac4C in polyA RNA samples. Both the ac4C (or C) and m6A (or A) peaks can be detected by the chromatograms in the standard samples but not in the blank solution (Figure 1D-G). The polyA RNA purified from the HOM of mouse hippocampus showed ac4C peaks with a stoichiometry level of 0.426 ± 0.049% (n = 3 biological replicates) (Figure 1H). Likewise, the polyA RNA

88 purified from the HOM of mouse hippocampus showed m6A peaks with a
89 stoichiometry level of 0.223 ± 0.046% (n = 3 biological replicates) (Figure 1I), which
90 is consistent with the previous study form mouse brain[37]. When the polyA RNA samples
91 were incubated with 50 mM NH_2OH for 1 h before LC-MS/MS, a protocol of chemical
92 deacetylation[38], the stoichiometry levels of ac4C were significantly reduced (Figure
93 1H), indicating the validity of the LC-MS/MS analysis. By contrast, the stoichiometry
94 levels of m6A in polyA RNA samples remained unchanged after NH_2OH treatment
95 (Figure 1I), supporting the specificity of the deacetylation protocol. Altogether these
96 results demonstrate the presence of ac4C modification in polyA RNA from mouse
97 hippocampus. Given that polyA RNA consists of mRNA and long noncoding RNA
98 (lncRNA)[39], we further performed acRIP-seq to analyze the ac4C mRNA in mouse
99 hippocampus.

100 **Characterization of ac4C mRNA in the HOM of mouse hippocampus after**
101 **memory**

102 We used the behavioral protocol of MWM[40] to study how memory regulate mRNA
103 acetylation in mouse hippocampus. The control mice were placed in the MWM with a
104 visible platform once a day for 2 days, and thus could reach the visible platform in the
105 target region without training (Figures S1A and S1B). However, the control mice could
106 not remember the target region during the probe test at day 6 (Figures S1A and S1C).
107 In contrast, the learning mice were subjected to training in the MWM with a hidden
108 platform (Figures S1D and S1E). The learning mice took 5 days of training to remember
109 the target region during the probe test at day 6 (Figures S1E and S1F), indicative of
110 memory. Consistent with the previous study[41], the learning mice could not remember
111 the target region during the probe test at day 20 after staying in the home cages for 2
112 weeks without training (Figures S1D and S1G), indicating that memories were naturally
113 forgotten (Figures S1H).

114 We next performed acRIP-seq[19] to identify ac4C mRNA in the HOM of mouse
115 hippocampus. Two libraries of RNA (acRIP and input) were subjected to the next-
116 generation sequencing (NGS) for each sample (Table S1). The acRIP-seq reads were

mapped to mouse hippocampal transcriptome to identify ac4C enriched regions relative to input, and the fold enrichment (FE) of an ac4C peak was defined as acRIP / input (Figure S2A). An ac4C peak was considered positive when its FE > 2 and adjusted p-values < 0.05[42].

We performed acRIP-seq for three HOM replicates from control and learning mice one hour after probe tests in the MWM (i.e., at day 6). The ac4C peaks and ac4C mRNAs identified in three biological replicates of control and learning mice were largely overlapped (Figures S2B and S2C). These results indicate the consistency of the acRIP-seq for mouse hippocampus. The ac4C peak that were identified from at least two of the three biological replicates were considered reliable. Only mRNAs corresponding to these reliable ac4C peaks are defined as reliably ac4C mRNAs. We identified 14516 ac4C peaks and 8303 ac4C mRNAs from the HOM of control mice (Figure S2B and Table S2), and 13348 ac4C peaks and 8107 ac4C mRNAs from the HOM of learning mice (Figures S2C and Table S2). Moreover, the acRIP-seq revealed the same consensus motif AGCAGCTG in the ac4C peak regions from three biological replicates of control and learning mice (Figure S2D).

When we compared the transcripts with ac4C modifications to the entire transcriptome, we found that 54.1 ± 2.62% (n = 3 biological replicates) of the mRNAs in the mouse hippocampus were modified by ac4C. In line with the previous study from Hela cells[19], metagene profile analysis revealed that most ac4C peaks were located within the coding sequence (CDS) of mRNAs in mouse hippocampus, with lower density in the 5' and 3' untranslated regions (Figures S2E and S2F). To further assess the reproducibility of our ac4C detection, we performed Upset plot analysis which revealed 4,494 peaks common to all three biological replicates in control mice and 4,110 peaks in learning mice (Figures S2G and S2H). The comparable overlap patterns between control and learning conditions confirm the stability of global ac4C modification patterns following memory formation. The numbers of ac4C peak per acetylated mRNA were comparable across three biological replicates and between control and learning mice (Figure S2I). Likewise, the ac4C dot-blots of polyA RNA,

and the cumulative distribution of ac4C mRNAs in the HOM were similar between the control and learning mice (Figures S2J and S2K). The cumulative distribution of mRNA counts in the HOM that were revealed by the NGS of input RNA were also similar between control and learning mice (Figure S2L). Altogether these results suggest that the total levels of ac4C mRNA in the HOM of mouse hippocampus may not be altered by memory.

Dynamic change of ac4C polyA RNA in the SYN of mouse hippocampus during memory

We next purified the SYN fraction from mouse hippocampus, enriched for synaptic proteins (PSD95 and synapsin 1) and depleted of cytoplasm (the S2 fraction)-restricted protein (α-tubulin) (Figure 2A). We then analyzed the levels of ac4C polyA RNA purified from the SYN with the ac4C dot-blots. The control and learning mice showed similar levels of ac4C polyA RNA in the SYN at day 1 (Figure 2B). Strikingly, the levels of ac4C polyA RNA showed a significant increase in the SYN of learning mice at day 6, compared with controls (Figure 2C). However, the levels of ac4C polyA RNA returned to control levels in the SYN of learning mice at day 20 (Figure 2D). These results suggest that acetylation of polyA RNA was upregulated in the SYN of mouse hippocampus during memory but returned to control levels after memory forgetting. The dynamic change of ac4C RNA in the SYN of mouse hippocampus during memory was verified by the assay of LC-MS/MS (Figure 2E).

Characterization of ac4C mRNA in the SYN of mouse hippocampus

Given that the amount of RNA that could be purified from SYN (200 ng per mouse hippocampus) is much less than that from HOM (50 μg per mouse hippocampus), we used the protocol of low-input acRIP-seq to identify ac4C mRNAs in the SYN (see details in the Methods). Due to the limited yield of SYN RNA, we purified the SYN RNA from the hippocampus of 10 adult mice and combined them into one sample. Six total samples from control and learning mice at days 1, 6, and 20 were subjected to low-input acRIP-seq. Two libraries (acRIP and input) were sequenced for each sample (Table S1). To increase the data reliability for low-input acRIP-seq, transcripts that were

identified in our own sequencing and at least two of the three synaptosome databases[43-45] were considered reliable and included in the analysis.

The transcripts and ac4C mRNAs identified from the SYN of control and learning mice at days 1, 6 and 20 were largely overlapped (Figures S3A-B and S3E-F; Table S3). We found that 58.61 ± 1.39% of the mRNAs in the SYN from control mouse hippocampus were modified by ac4C. On average, every acetylated transcript had 1.77 ± 0.05 ac4C peaks in the SYN from control mouse hippocampus. Moreover, the low-input acRIP-seq revealed the same consensus motif AGCAGCTG in the ac4C peak regions of SYN mRNA from control and learning mice at days 1, 6 and 20 (Figure S3C and S3G). In line with the results from HOM, most ac4C peaks were identified in CDS of SYN mRNA from both control and learning mice (Figures S3D and S3H). These results indicate the consistency of the low-input acRIP-seq for SYN mRNA.

Dynamic change of ac4C mRNA in the SYN of mouse hippocampus during memory

The cumulative distribution of ac4C mRNAs in the SYN did not differ between control and learning mice at day 1 (Figure 2F). In contrast, the cumulative distribution curve of ac4C mRNAs in the SYN of learning mice had a significant rightward shift at day 6, compared with control mice (Figure 2G). Intriguingly, the cumulative distribution of ac4C mRNAs in the SYN of learning mice became indistinguishable from that of control mice at day 20 (Figure 2H). The cumulative distribution of mRNA counts in the SYN were similar between control and learning mice at days 1, 6, and 20 (Figures 2I-2K). These results suggest that acetylation of mRNA rather than the total levels of mRNA was increased in the SYN after memory, and mRNA acetylation returned to control levels after memory forgetting, supporting the dynamic change of acetylation of polyA RNA in the SYN during memory (Figures 2B-2E).

To further validate the distinct molecular characteristics of the “learning-day6” group, we performed principal component analysis (PCA) based on global ac4C modification profiles. The first two principal components accounted for 38% and 26% of the total variance, respectively. The “learning-day6” samples clustered distinctly

from the other five groups, confirming a unique epitranscriptomic signature associated with memory (Figures S3I). To identify the memory-induced synaptic ac4C (MISA) mRNA, we analyzed the fold change (FC) of ac4C mRNA in the SYN of learning versus control mice (L/C) at days 1, 6, 20 (Figures S3J-S3L). Here we analyzed the FE of all ac4C peaks to better reflect the acetylation level of individual mRNA. Acetylation of MISA mRNA should be upregulated after memory and return to control levels after memory forgetting. In other words, the ac4C of MISA mRNA should be upregulated specifically at day 6 (the cutoff value of upregulation is FC > 2) but not at days 1 or 20. Per these criteria, we identified 1237 MISA mRNAs whose ac4C levels were increased at day 6 rather than at days 1 or 20 in learning mice, compared with controls (Figure S3M; Table S4). In contrast, the transcription levels of MISA mRNAs were similar at days 1, 6, and 20 between control and learning mice (Figure S3I; Table S4).

A representative MISA mRNA for Arc

Gene ontology (GO) analysis indicated that MISA mRNAs were significantly enriched in the biological processes (BP) related with synaptic plasticity and learning or memory (Figure 3A; Table S4). Protein-protein interaction (PPI) network analysis of MISA mRNAs involved in learning or memory revealed several core genes such as activity-regulated cytoskeleton associated protein (Arc), glutamate receptor NMDA type subunit 1 (Grin1), and presenilin 1 (Psen1) (Figures 3A and 3B). ARC protein can be transported into dendrites and translated near activated postsynaptic sites after neural activities[46,47]. Different from other immediately early genes (IEG), Arc underwent repetitive cycles of transcription and local translation, which is critical for memory consolidation[48,49]. Although Arc is a promising “master regulator” of protein synthesis-dependent forms of memory, the mechanisms underlying the regulation of local translation of Arc in the SYN remained to be elucidated[50]. Analysis of the acRIP-seq data indicate that learning mice have elevated ac4C Arc mRNA in the SYN at day 6 rather than days 1 or 20, and similar levels of ac4C Arc mRNA in the HOM at day 6, compared with control mice (Figure 3C). The genome browser tracks for the ac4C of all MISA mRNAs were accessible at the ac4C website (http://ac4catlas.com/) to show

altered ac4C in the SYN, and similar lack of change for those same RNAs in the HOM at day 6.

Next, we used an orthogonal method to verify the dynamic change of ac4C Arc mRNA in the SYN during memory. To this end, performed RT-qPCR analysis for Arc mRNA from the input and acRIP samples from the SYN. The levels of input and acRIP-Arc mRNA were similar in the SYN of control and learning mice at days 1 and 20 (Figures 3D, 3E, 3G and 3H). Likewise, the protein levels of ARC were also comparable in the SYN of control and learning mice at days 1 and 20 (Figures 3F and 3I). Although the levels of input Arc mRNA were not altered in the SYN of learning mice at day 6 (Figure 3J), the levels of acRIP-Arc mRNA and ARC proteins were significantly increased in the SYN of learning mice at day 6, compared with controls (Figures 3K and 3L). In contrast, the levels of Arc mRNA and ARC proteins were similar in the HOM of control and learning mice at day 6 (Figures 3M and 3N). Note that Arc mRNA levels in the IgG-IP samples were much lower than that in the acRIP samples (Figures 3E, 3H and 3K), indicating the specificity of RT-qPCR for acetylated Arc mRNA. Altogether the results demonstrate that acetylation of Arc mRNA is specifically increased in the SYN after memory but returned to control levels after memory forgetting.

Expression of Nat10 in the mature neurons of mouse hippocampus

NAT10 is the only known ac4C writer[21]. Since the commercially available NAT10 antibodies were not suitable for immunostaining in the hippocampal slices, we took use of the strategy of genetic labeling[51,52] to investigate the expression pattern of Nat10. To this end, a heterozygous knockin mouse line ($Nat10^{Cre/+}$) that expressed the Cre recombinase right after the start codon (ATG) of Nat10 gene was generated using the CRISPR/Cas9 techniques (see details in the Method). Since the Cre recombinase and Nat10 share the same regulatory elements for gene expression in the $Nat10^{Cre/+}$ mice, the Nat10 expression pattern can be revealed through the Cre-reporting adeno-associated virus (AAV) that express EGFP in a Cre-dependent manner. In this way, the Nat10-positive cells would express EGFP in the Nat10 reporter mice (Figure 4A).

The dorsal hippocampus integrates multiple synaptic inputs from other brain regions, and is critical for learning and memory[53-55]. To study the expression pattern of Nat10 in the dorsal hippocampus of adult mice, we injected Cre-reporting AAV into the dorsal hippocampus of 7-week-old Nat10$^{Cre/+}$ mice, and the fluorescent protein EGFP was analyzed 3 weeks after AAV injection. Analysis of the EGFP-positive cells revealed that Nat10 was mainly expressed in the pyramidal cell layer (sp) of CA1 region and granule cell layer (gcl) of dentate gyrus (DG) (Figure 4B). Around 80% of Nat10-expressing cells are mature neurons, evidenced by the overlay between EGFP and NeuN, a protein marker for mature neurons (Figures 4C and 4D). Note that about 20% of Nat10-positive cells are non-neuronal and probably glia cells. Moreover, about 75% of Nat10-positive cells are excitatory pyramidal neurons in the CA1 region of mouse hippocampus, indicated by the co-localization of EGFP with Neurogranin (NG), a protein marker for excitatory pyramidal neurons (Figures 4C and 4E). Collectively these results indicate that Nat10 is mainly expressed by mature neurons in adult mouse hippocampus.

To generate Nat10-reporter mice, Nat10-Cre mice were crossed with Ai14 tdTomato reporter mice, leading to tdTomato expression in Nat10-expressing cells. To validate the neuronal expression pattern of Nat10, we utilized Nat10-reporter mice and observed tdTomato signals predominantly in neurons within the CA1 region (Figure 4F and 4G). Collectively, these results demonstrate that Nat10 is primarily expressed in mature neurons.

Increase of NAT10 proteins in the SYN after memory

The above-mentioned data showed that the levels of ac4C mRNA were increased in the SYN of mouse hippocampus after memory. Next, we aim to investigate whether the protein levels of NAT10, the only known ac4C writer[21], are also regulated by memory. Toward this aim, we purified the SYN fraction from the hippocampus of control and learning mice at days 1, 6 and 20, and analyzed the protein levels of NAT10 by western blots (Figure 5A). The protein levels of NAT10 in the SYN were similar between control and learning mice at day 1 (Figure 5B). Interestingly, the protein levels of

291 NAT10 were significantly increased in the SYN of learning mice at day 6 (Figure 5C),
292 but returned to control levels at day 20 (Figure 5D). These results indicate that protein
293 levels of NAT10 are increased in the SYN after memory but return to normal levels
294 after memory forgetting (Figure 5E).

295 The protein levels of NAT10 were not altered in HOM of learning mice at day 6,
296 compared to controls (Figure 5F), suggesting that memory did not upregulate the de
297 novo protein synthesis of NAT10 in mouse hippocampus. To further explore the
298 distribution of NAT10 proteins in other subcellular fractions, we purified the nucleus
299 (N), cytoplasm (S2) and post-synaptic density (PSD) fractions from the hippocampus
300 of control and learning mice at day 6, and analyzed the protein levels of NAT10 in
301 different subcellular fractions (Figure 5G). The nuclear fraction was enriched for
302 histone but was depleted of cytoplasmic protein α-tubulin or synaptic protein SYN1
303 and PSD95, and vice versa for the S2 and PSD fractions (Figure 5H). The protein levels
304 of NAT10 in the nucleus did not change at day 6 after memory (Figure 5I). Strikingly,
305 the NAT10 proteins were significantly reduced in the cytoplasm (S2 fraction) but
306 increased in the PSD fraction at day 6 after memory (Figures 5J and 5K). These results
307 suggest that NAT10 proteins might be relocated from the cytoplasm to synapses in
308 mouse hippocampus after memory.

309 NAT10 belongs to the p300/CBP-associated factor (PCAF) subfamily of protein
310 acetyltransferase[56]. Next, we aim to investigate whether memory changed protein levels
311 of PCAF in the subcellular fractions of mouse hippocampus. The protein levels of
312 PCAF did not change in the nucleus, cytoplasm or PSD fractions of learning mice at
313 day 6, compared to controls (Figures 5L-5N), indicating that memory may not alter the
314 subcellular distribution of PCAF.

315 Next, we performed immunofluorescent staining to study the synaptic distribution
316 of NAT10 proteins before and after chemical LTP stimulation in cultured hippocampal
317 neurons (Figure S4A) – a cellular model of learning and memory[57,58]. In control neurons
318 treated with vehicle, NAT10 was mainly expressed in the nucleus and cytoplasm
319 (Figure S4B), which is consistent with the results of western blots (Figures 5I-5J).

However, 60 minutes after chemical LTP stimulation, the colocalization of NAT10 with PSD95, a protein marker for PSD fraction, was significantly increased, compared with control neurons (Figures S4C-S4D). These results indicated that distribution of NAT10 in the PSD were increased in hippocampal neurons after chemical LTP stimulation, which is consistent with the upregulation of NAT10 in the synapse of mouse hippocampus after memory (Figure 5).

NAT10-dependent ac4C polyA RNA in mouse hippocampus

To demonstrate the NAT10-dependent ac4C modification of poly A RNA, we used the Cre/Loxp strategy[59] to downregulate Nat10 expression in adult mouse hippocampus through injection of AAV-EGFP-P2A-Cre into the hippocampus of $Nat10^{flox/flox}$ mice. Given that Nat10 is mainly expressed in the mature neurons (Figure 4), the expression of EGFP-2A-Cre in the AAV was driven by the human synapsin 1 (Syn1) promoter, a neuron-specific promoter[60]. The $Nat10^{flox/flox}$ mice injected with AAV-EGFP and AAV-EGFP-P2A-Cre were named control and Nat10 conditional knockout (cKO) mice hereafter. Both the control and Nat10 cKO mice received stereotaxic AAV injection into the dorsal hippocampus, and the HOM of dorsal hippocampus were collected for biochemical assay 3 weeks after AAV injection (Figure S5A).

The fluorescent protein EGFP was expressed mainly in the CA1-3 regions and DG of mouse hippocampus 3 weeks after AAV injection (Figure S5B), indicating the successful infection of AAV. The protein levels of NAT10 were significantly reduced in the hippocampus of Nat10 cKO mice, compared with controls (Figures S5C and S5D), verifying the effective knockdown of NAT10 by the Cre/Loxp strategy. NAT10 was previously described as a protein acetyltransferase against α-tubulin and histones[61,62]. However, immunoblotting with acetylation-specific antibodies showed no significant change of protein acetylation in Nat10 cKO hippocampus, compared to controls (Figures S5C, S5E and S5F). These results suggest the redundancy of acetyltransferases for α-tubulin and histones in mouse hippocampus. In contrast, the ac4C modification of polyA RNA was significantly decreased in the hippocampus of Nat10 cKO mice, compared with controls (Figures S5G and S5H). As a control experiment,

349 downregulation of NAT10 did not affect the m6A modification of polyA RNA (Figures
350 S5I and S5J). The LC-MS/MS analysis of polyA RNA indicated that the stoichiometry
351 levels of ac4C rather than m6A were significantly reduced in the hippocampus of Nat10
352 cKO mice, compared with controls (Figures S5K and S5L). The partial reduction of
353 ac4C in the Nat10 cKO mice might be due to the limited infection areas of Cre-AAV,
354 or the Nat10 expression in non-neuronal cells, or the presence of other unknown ac4C
355 writers. Nonetheless, these results demonstrate that NAT10 specifically regulates ac4C
356 rather than m6A modification of polyA RNA in mouse hippocampus.

357 **NAT10-dependent ac4C mapping of SYN mRNA in learning mice**

358 Given that memory increased ac4C mRNA specifically in the SYN, we next aim to
359 identify NAT10-dependent ac4C modification of synaptic mRNAs. To this end, we
360 performed low-input acRIP-seq for SYN RNA purified from the hippocampus of
361 control and Nat10 cKO mice at day 6 after memory (Figure S6A). Due to the limited
362 yield of SYN RNA, we purified SYN RNA from the hippocampus of 10 mice and
363 combined them into one sample. Two biological samples from control and Nat10 cKO
364 mice at day 6 were subjected to low-input acRIP-seq to demonstrate the NAT10-
365 dependent ac4C modification of SYN mRNA. Two libraries (acRIP and input) were
366 sequenced for each biological sample (Table S3).

367 We identified 7097 and 1933 ac4C peaks from the SYN of control and Nat10 cKO
368 mice, respectively (Figure S6B). These results suggest a reduction of the a4C peak
369 number by knockout of Nat10 in mature neurons of adult mouse hippocampus. Out of
370 7097 ac4C peaks identified in control mice, 6331 peaks were abolished and 408 peaks
371 were downregulated in Nat10 cKO mice, and these ac4C peaks were named NAT10-
372 dependent synaptic ac4C (NASA) peaks (Figure S6C) which were mainly localized in
373 the CDS region of mRNA (Figure S6D)

374 The Nat10 cKO mice also showed a reduction of ac4C mRNA number in the SYN,
375 compared with controls (Figure S6E). In contrast, the number of mRNA in the SYN
376 was similar between control and Nat10 cKO mice (Figure S6F). Likewise, the levels of
377 ac4C mRNA rather than total mRNA were significantly reduced in the SYN of Nat10

cKO mice, compared with controls, evidenced by the leftward-shifted cumulative distribution curve of FE of ac4C mRNA in the Nat10 cKO mice (Figures 6A-6C). Out of 3,778 ac4C-modified mRNAs identified in the SYN of control mice, 2,507 were classified as diminished, indicating that their ac4C enrichment fell below the detection threshold or became undetectable in Nat10 cKO mice (FE < 1 or peak lost). An additional 839 mRNAs were downregulated, defined as showing significantly reduced but still detectable ac4C levels in cKO mice compared to controls. Collectively, these transcripts were referred to as NASA mRNAs (Figure S6G; Table S5). Analysis of the overlap between MISA and NASA indicated that 717 out of 1237 MISA mRNAs were regulated by NAT10 (Figure 6D).

We next analyzed the cellular expression pattern of NASA mRNAs through the single-cell RNA-seq atlas of mouse hippocampus (dropviz.org)[63]. The results indicated that the expression of NASA mRNAs was mostly enriched in excitatory neurons (Figure S6H), which is in line with the cellular expression pattern of NAT10 in mouse hippocampus (Figure 4). In addition, about 13% of NASA mRNAs were relatively enriched in glia cells (Figure S6H), which is consistent with the notion that processes of glia cells contribute to formation of the tripartite synapses[64,65].

Regulation of ac4C and protein levels of memory-related mRNAs by NAT10

Arc, a representative MISA mRNA (Figure 3), is critical for memory[66]. The mRNA of Ca^{2+}/calmodulin-dependent protein kinase 2α (Camk2α) and Grin 2b encode the protein kinase CaMKIIα and the GluN2B subunit of NMDA receptor, respectively. CaMKIIα and GluN2B are synapse-enriched proteins and play important roles in LTP as well as memory[67,68]. Recent studies demonstrate that CaMK2α interaction with GluN2B is critical for the induction and maintenance of LTP[69,70]. Analysis of the low-input acRIP-seq data indicated the reduction of ac4C peaks of Arc, Camk2α and Grin 2b mRNAs in the SYN of Nat10 cKO mice, compared with controls (Figures 6E-6G). The genome browser tracks for the ac4C of all NASA mRNAs were accessible at the ac4C website (http://ac4catlas.com/) to show reduced or diminished ac4C peaks in the SYN of Nat10 cKO mice, compared with controls. Despite the presence of a common

AGCAGCTG motif in both groups, Nat10 deletion disrupted the local CXX sequence context, reflecting a shift in ac4C deposition specificity upon loss of Nat10 enzymatic activity (Figures S6I). Moreover, BP enrichment of the 717 shared ac4C-modified mRNAs revealed significant enrichment in biological processes such as synapse organization and dendrite development, indicating a potential role of ac4C modification in regulating synaptic structure and neuronal connectivity (Figures S6J).

Next, we performed RT-qPCR analysis for input and acRIP RNAs purified from the SYN of control and Nat10 cKO mice at day 6 after memory to verify the NAT10-dependent ac4C modification of Arc, Camk2α and Grin2b mRNAs. The input mRNA levels of Arc, Camk2α and Grin2b in the SYN were comparable between control and Nat10 cKO mice (Figure 6H). In contrast, the acRIP mRNA levels of Arc, Camk2α and Grin2b in the SYN were significantly reduced in Nat10 cKO mice, compared with controls (Figure 6I). Given that ac4C modification of mRNA has been shown to enhance translation efficiency[19,20], we sought to determine whether NAT10 influences the protein levels of ARC, CaMKIIα and GluN2B in the SYN by western blot analysis. The protein levels of ARC, CaMKIIα and GluN2B were significantly decreased in the SYN at day 6 from Nat10 cKO mice, compared with controls (Figure 6J). Altogether, these results demonstrate that NAT10 regulates ac4C and protein levels of Arc, Camk2α and Grin2b in the SYN of mouse hippocampus at day 6.

Regulation of LTP as well as memory by NAT10 in mouse hippocampus

In the following study, we investigate whether NAT10 in mouse hippocampus is important for synaptic plasticity. The body and brain weight were similar between control and Nat10 cKO mice (Figures S7A and S7B). The number and intrinsic excitability of CA1 pyramidal neurons were also comparable between control and Nat10 cKO mice (Figures S7C and S7D). To address whether NAT10 regulates LTP, we performed electrophysiology recording of fEPSP (field excitatory postsynaptic potential) at the SC-CA1 synapses before and after high frequency stimulation (HFS) (Figure 7A). The induction of LTP was comparable between control and Nat10 cKO mice (Figures 7B-7E). However, the maintenance of LTP especially the late phase of

436 LTP was severely impaired in Nat10 cKO mice, compared with controls (Figures 7B,
437 7C and 7F).

438 To further study whether Nat10 is important for synaptic plasticity after memory,
439 we performed fEPSP recording to investigate glutamatergic transmission at the SC-
440 CA1 synapses in the control and Nat10 cKO mice at day 6 (Figure 6G). Consistent with
441 the previous report[71], the glutamatergic transmission at the SC-CA1 synapses was
442 significantly enhanced at day 6 in learning mice, compared with mice without learning
443 (Figures 7H and 7I). The glutamatergic transmission at the SC-CA1 synapses was
444 similar between control and Nat10 cKO mice without learning, which indicate that
445 Nat10 may be dispensable for the basal glutamatergic transmission at the SC-CA1
446 synapses. However, the memory-induced enhancement of glutamatergic transmission
447 at the SC-CA1 synapses was significantly impaired in Nat10 cKO mice, compared with
448 controls (Figures 7H and 7I). Altogether these results indicate that NAT10 is important
449 for synaptic plasticity related with memory in mouse hippocampus.

450 To investigate whether NAT10 is critical for memory, both control and Nat10 cKO
451 mice were subjected to training in the MWM for 5 days, and the probe test was
452 performed at day 6. Both groups exhibited an overall decline in the latency to reach the
453 platform at the early stage (day 1-2) of training (Figure 7J). However, the Nat10 cKO
454 mice failed to improve performance during the late training stage (day 3-5), compared
455 with controls (Figure 7J). During the probe tests, the control and Nat10 cKO mice
456 showed similar distance travelled (Figures 7K and 7L). However, the time spent in the
457 target area and the number of platform crossing were significantly reduced in the Nat10
458 cKO mice, compared with controls (Figures 7L-7N). These results demonstrate that
459 NAT10 in mouse hippocampus is important for spatial memory.

460

461 **Discussion**

462 In this study, we demonstrate the dynamic regulation of synaptic mRNA acetylation by
463 memory in mouse hippocampus. We identified ~1200 MISA mRNAs that were
464 increased in the SYN of mouse hippocampus after memory but returned to normal

levels after memories were naturally forgotten. Interestingly, the protein levels of NAT10 were also increased in the SYN after memory but returned to control levels after forgetting. We further showed NAT10-dependent ac4C mapping of SYN mRNAs through the acRIP-seq and verified the NAT10-dependent ac4C modification of Arc, Camk2α and Grin2b mRNAs. The maintenance of LTP at the SC-CA1 synapses as well as the behaviors of memory were severely impaired in the Nat10 cKO mice. In support of the importance of ac4C in memory, our recent study showed that ac4C modification of several MISA mRNAs including Arc, Grin1 and Psen1 was significantly reduced in the hippocampus of 5×FAD mouse, an animal model of Alzheimer's disease that was characterized by deficient synaptic plasticity and memory[72]. Altogether these results demonstrate the importance of NAT10-mediated mRNA acetylation in memory.

The dynamic regulation of protein acetylation in the SYN by memory has been shown in our previous studies[73-76]. In contrast to the well-characterized acetyltransferases and deacetylases for protein acetylation[77], the writer and eraser of mRNA acetylation are less well understood. The NAT10 acetyltransferase is the only known ac4C writer in the mammalian cells[24,78]. Recently, the deacetylase SIRT7 has been shown to erase the ac4C modification of ribosomal RNA (rRNA) and small nucleolar RNA (snoRNA)[79,80]. However, the mechanisms underlying the deacetylation of mRNA need further exploration.

How the ac4C modification of mRNA is regulated by neural activities remains largely unknown. Our previous studies showed that overnight starvation downregulated the ac4C modification of tyrosine hydroxylase (TH) mRNA in the sympathetic nerve terminus that innervate the olfactory mucosa in mice, which reduced TH protein levels and dopamine synthesis in the mouse olfactory mucosa after overnight starvation[81]. In this study, we demonstrate that memory regulate the dynamic change of ac4C modification of mRNA at synapses of mouse hippocampus. Altogether these studies provide evidence that neural activities regulate acetylation of mRNA in a spatiotemporally specific manner.

NAT10 proteins were increased in the SYN but reduced in the cytoplasm of mouse

494 hippocampus at day 6 in the MWM. These results suggest a relocation of NAT10 from
495 the cytoplasm to synapses after memory, which was corroborated by the
496 immunostaining study of NAT10 distribution in cultured mouse hippocampal neurons
497 after cLTP stimulation. Previous proteomic studies showed that NAT10 were detected
498 in the interactome with several motor proteins such as kinesin proteins[82], which raised
499 the possibility that NAT10 might be transported by the motor proteins in hippocampal
500 neurons during memory. NAT10 was highly expressed in the nucleus of hippocampal
501 neurons, but protein levels of nuclear NAT10 were not altered at day 6 in the MWM.
502 NAT10 has been shown to be important for regulating nuclear functions such as
503 nucleolar assembly[62] and nuclear architecture[83]. The function of NAT10 in the nucleus
504 of neurons waits for future investigations.

505 The subcellular change of NAT10 proteins at day 6 apparently may not be caused
506 by stress during the training in the MWM. The mice were well handled before and
507 during the training, and thus the stress should be minor if any. The control mice were
508 exposed to the training using visible platform at day 1, the stress levels in the control
509 mice may be vary with the learning mice. If mild stress during the training in the MWM
510 could cause the relocation of NAT10 to the SYN, the protein levels of NAT10 in the
511 SYN would be increased at day 1. However, the protein levels of NAT10 in the SYN
512 were similar at day 1 between control and learning mice. In addition, chronic mild stress
513 has been shown to increase the total protein levels of NAT10 in mouse hippocampus[84].
514 In contrast, the total protein levels of NAT10 in mouse hippocampus did not alter at day
515 6 in the MWM. These results suggest that the increased NAT10 proteins in the SYN at
516 day 6 in the MWM may be related with memory rather than stress.

517 The stoichiometry levels of ac4C in polyA RNA has been reported to be ~0.2% in
518 HeLa cells[19], ~0.1% in human embryonic stem cells[24], ~0.2% in liver[85], and ~0.3% in
519 heart[25]. Here we showed that ~0.4% of cytidine was acetylated in mouse hippocampus.
520 Although the total protein levels of NAT10 has been reported to be relatively lower in
521 the whole brain tissue compared with reproductive tissues such as testis and ovary[26],
522 the NAT10 was shown to be highly expressed in hippocampal neurons[86]. Future studies

are warranted to investigate how the acetyltransferase activity of NAT10 toward mRNA was regulated in different brain regions and different tissues.

The basal glutamatergic transmission at the SC-CA1 synapses were unaltered in the Arc knockout mice[87], which is consistent with the phenotypes in the Nat10 cKO mice. On the other hand, ARC has been shown to accelerate AMPA receptor endocytosis[88], and thus the induction of LTP at the SC-CA1 synapses was enhanced in the Arc knockout mice[87]. Although ARC protein levels were decreased in the SYN of Nat10 cKO mice, the induction of LTP at the SC-CA1 synapses was not increased in the Nat10 cKO mice, which might be due to the reduction of other LTP-promoting proteins such as CaMKIIα and GluN2B in the SYN of Nat10 cKO mice.

In line with the phenotypes of Nat10 cKO mice presented in this study, the Arc knockout mice showed deficits in the late phase of LTP at SC-CA1 synapses and impairment of memory consolidation in the MWM[87]. Consistent with the function of Arc in memory consolidation, the acetylation of Arc mRNA was increased in the SYN at day 6 rather than day 1 following MWM training, a period during which memories were consolidated. Moreover, the increase of ac4C and protein levels of Arc in the SYN at day 6 was NAT10-dependent, which might underlie the contribution of NAT10 in memory. In Figure 3A, GO enrichment analysis revealed a significant association with the term “regulation of protein stability.” This raises the possibility that the increased ARC protein levels observed in Nat10 cKO mice may not be solely due to enhanced mRNA stability, but could also reflect reduced protein degradation. Although our current study primarily focuses on the role of ac4C in mRNA stability, we cannot exclude the possibility that Nat10 deficiency also affects post-translational regulatory pathways. However, the function of NAT10 in regulating tRNA or rRNA might also contribute to memory. New techniques for overexpression and erasure of site-specifically acetylated mRNA need to be developed to precisely study the function of mRNA acetylation. Nonetheless, the results presented here provide evidence that NAT10-mediated mRNA acetylation may contribute to the protein synthesis at synapses during memory in mouse hippocampus.

References

1. Shrestha, P., and Klann, E. (2022). Spatiotemporally resolved protein synthesis as a molecular framework for memory consolidation. Trends Neurosci 45, 297-311. https://doi.org/10.1016/j.tins.2022.01.004.
2. Besse, F., and Ephrussi, A. (2008). Translational control of localized mRNAs: restricting protein synthesis in space and time. Nat Rev Mol Cell Biol 9, 971-980. https://doi.org/10.1038/nrm2548.
3. Martin, K.C., Barad, M., and Kandel, E.R. (2000). Local protein synthesis and its role in synapse-specific plasticity. Curr Opin Neurobiol 10, 587-592. https://doi.org/10.1016/s0959-4388(00)00128-8.
4. Sutton, M.A., and Schuman, E.M. (2006). Dendritic protein synthesis, synaptic plasticity, and memory. Cell 127, 49-58. https://doi.org/10.1016/j.cell.2006.09.014.
5. Day, J.J., and Sweatt, J.D. (2011). Epigenetic mechanisms in cognition. Neuron 70, 813-829. https://doi.org/10.1016/j.neuron.2011.05.019.
6. Levenson, J.M., and Sweatt, J.D. (2005). Epigenetic mechanisms in memory formation. Nat Rev Neurosci 6, 108-118. https://doi.org/10.1038/nrn1604.
7. Fischer, A., Sananbenesi, F., Wang, X., Dobbin, M., and Tsai, L.-H. (2007). Recovery of learning and memory is associated with chromatin remodelling. Nature 447, 178-182. https://doi.org/10.1038/nature05772.
8. Levenson, J.M., O'Riordan, K.J., Brown, K.D., Trinh, M.A., Molfese, D.L., and Sweatt, J.D. (2004). Regulation of histone acetylation during memory formation in the hippocampus. J Biol Chem 279, 40545-40559. https://doi.org/10.1074/jbc.M402229200.
9. Kouzarides, T. (2007). Chromatin modifications and their function. Cell 128, 693-705. https://doi.org/10.1016/j.cell.2007.02.005.
10. Merkurjev, D., Hong, W.-T., Iida, K., Oomoto, I., Goldie, B.J., Yamaguti, H., Ohara, T., Kawaguchi, S.-y., Hirano, T., and Martin, K.C. (2018). Synaptic N 6-methyladenosine (m6A) epitranscriptome reveals functional partitioning of localized transcripts. Nat Neurosci 21, 1004-1014. https://doi.org/10.1038/s41593-018-0173-6.
11. Zhuang, M., Geng, X., Han, P., Che, P., Liang, F., Liu, C., Yang, L., Yu, J., Zhang, Z., Dong, W., and Ji, S.-J. (2023). YTHDF2 in dentate gyrus is the m6A reader mediating m6A modification in hippocampus-dependent learning and memory. Mol Psychiatry 28, 1679-1691. https://doi.org/10.1038/s41380-023-01953-z.
12. Shi, H., Zhang, X., Weng, Y.-L., Lu, Z., Liu, Y., Lu, Z., Li, J., Hao, P., Zhang, Y., Zhang, F., et al. (2018). m6A facilitates hippocampus-dependent learning and memory through YTHDF1. Nature 563, 249-253. https://doi.org/10.1038/s41586-018-0666-1.
13. Boccaletto, P., Machnicka, M.A., Purta, E., Piątkowski, P., Bagiński, B., Wirecki, T.K., de Crécy-Lagard, V., Ross, R., Limbach, P.A., and Kotter, A. (2018). MODOMICS: a database of RNA modification pathways. 2017 update.

Nucleic Acids Res 46, D303-D307. https://doi.org/10.1093/nar/gkx1030.
14. Stern, L., and LH, S. (1978). The role of the minor base N4-acetylcytidine in the function of the Escherichia coli noninitiator methionine transfer RNA. J Biol Chem 17, 6132-6139. https://doi.org/10.1016/s0021-9258(17)34590-8.
15. Oashi, Z., Murao, K., Yahagi, T., Von Minden, D.L., McCloskey, J.A., and Nishimura, S. (1972). Characterization of C + located in the first position of the anticodon of Escherichia coli tRNA Met as N 4 -acetylcytidine. Biochim Biophys Acta 262, 209-213. https://doi.org/10.1016/0005-2787(72)90234-1.
16. Kowalski, S., Yamane, T., and Fresco, J.R. (1971). Nucleotide sequence of the "denaturable" leucine transfer RNA from yeast. Science 172, 385-387. https://doi.org/10.1126/science.172.3981.385.
17. Kruppa, J., and Zachau, H.G. (1972). Multiplicity of serine-specific transfer RNAs of brewer's and baker's yeast. Biochim Biophys Acta 277, 499-512. https://doi.org/10.1016/0005-2787(72)90093-7.
18. Ito, S., Akamatsu, Y., Noma, A., Kimura, S., Miyauchi, K., Ikeuchi, Y., Suzuki, T., and Suzuki, T. (2014). A single acetylation of 18 S rRNA is essential for biogenesis of the small ribosomal subunit in Saccharomyces cerevisiae. J Biol Chem 289, 26201-26212. https://doi.org/10.1074/jbc.M114.593996.
19. Arango, D., Sturgill, D., Alhusaini, N., Dillman, A.A., Sweet, T.J., Hanson, G., Hosogane, M., Sinclair, W.R., Nanan, K.K., and Mandler, M.D. (2018). Acetylation of cytidine in mRNA promotes translation efficiency. Cell 175, 1872-1886. e1824. https://doi.org/10.1016/j.cell.2018.10.030
20. Arango, D., Sturgill, D., Yang, R., Kanai, T., Bauer, P., Roy, J., Wang, Z., Hosogane, M., Schiffers, S., and Oberdoerffer, S. (2022). Direct epitranscriptomic regulation of mammalian translation initiation through N4-acetylcytidine. Mol Cell 82, 2797-2814. e2711. https://doi.org/10.1016/j.molcel.2022.05.016.
21. Ito, S., Horikawa, S., Suzuki, T., Kawauchi, H., Tanaka, Y., Suzuki, T., and Suzuki, T. (2014). Human NAT10 is an ATP-dependent RNA acetyltransferase responsible for N4-acetylcytidine formation in 18 S ribosomal RNA (rRNA). J Biol Chem 289, 35724-35730. https://doi.org/10.1074/jbc.C114.602698.
22. Liu, Y., Wang, X., Liu, Y., Yang, J., Mao, W., Feng, C., Wu, X., Chen, X., Chen, L., and Dong, P. (2023). N4-acetylcytidine-dependent GLMP mRNA stabilization by NAT10 promotes head and neck squamous cell carcinoma metastasis and remodels tumor microenvironment through MAPK/ERK signaling pathway. Cell Death Dis 14, 712. https://doi.org/10.1038/s41419-023-06245-6.
23. Wang, G., Zhang, M., Zhang, Y., Xie, Y., Zou, J., Zhong, J., Zheng, Z., Zhou, X., Zheng, Y., and Chen, B. (2022). NAT10 - mediated mRNA N4 - acetylcytidine modification promotes bladder cancer progression. Clin Transl Med 12, e738. https://doi.org/10.1002/ctm2.738.
24. Hu, Z., Lu, Y., Cao, J., Lin, L., Chen, X., Zhou, Z., Pu, J., Chen, G., Ma, X., and Deng, Q. (2024). N-acetyltransferase NAT10 controls cell fates via connecting

mRNA cytidine acetylation to chromatin signaling. Sci Adv 10, eadh9871. https://doi.org/10.1126/sciadv.adh9871.

25. Shi, J., Yang, C., Zhang, J., Zhao, K., Li, P., Kong, C., Wu, X., Sun, H., Zheng, R., and Sun, W. (2023). NAT10 is involved in cardiac remodeling through ac4C-mediated transcriptomic regulation. Circ Res 133, 989-1002. https://doi.org/10.1161/CIRCRESAHA.122.322244.

26. Jiang, X., Cheng, Y., Zhu, Y., Xu, C., Li, Q., Xing, X., Li, W., Zou, J., Meng, L., and Azhar, M. (2023). Maternal NAT10 orchestrates oocyte meiotic cell-cycle progression and maturation in mice. Nat Commun 14, 3729. https://doi.org/10.1038/s41467-023-39256-0.

27. Zhang, M., Yang, K., Wang, Q.-H., Xie, L., Liu, Q., Wei, R., Tao, Y., Zheng, H.-L., Lin, N., and Xu, H. (2023). The cytidine N-acetyltransferase NAT10 participates in peripheral nerve injury-induced neuropathic pain by stabilizing SYT9 expression in primary sensory neurons. J Neurosci 43, 3009-3027. https://doi.org/10.1523/JNEUROSCI.2321-22.2023.

28. Xu, T., Wang, J., Wu, Y., Wu, J.Y., Lu, W.C., Liu, M., Zhang, S.B., Xie, D., Xin, W.J., and Xie, J.D. (2023). Ac4C Enhances the Translation Efficiency of Vegfa mRNA and Mediates Central Sensitization in Spinal Dorsal Horn in Neuropathic Pain. Adv Sci 10, e2303113. https://doi.org/10.1002/advs.202303113.

29. Jarrard, L.E. (1993). On the role of the hippocampus in learning and memory in the rat. Behav Neural Biol 60, 9-26. https://doi.org/10.1016/0163-1047(93)90664-4.

30. Moser, M.-B., Trommald, M., and Andersen, P. (1994). An increase in dendritic spine density on hippocampal CA1 pyramidal cells following spatial learning in adult rats suggests the formation of new synapses. Proc Natl Acad Sci U S A 91, 12673-12675. https://doi.org/10.1073/pnas.91.26.12673.

31. Morris, R. (1984). Developments of a water-maze procedure for studying spatial learning in the rat. J Neurosci Methods 11, 47-60. https://doi.org/10.1016/0165-0270(84)90007-4.

32. Bliss, T.V., and Collingridge, G.L. (1993). A synaptic model of memory: long-term potentiation in the hippocampus. Nature 361, 31-39. https://doi.org/10.1038/361031a0.

33. Biever, A., Glock, C., Tushev, G., Ciirdaeva, E., Dalmay, T., Langer, J.D., and Schuman, E.M. (2020). Monosomes actively translate synaptic mRNAs in neuronal processes. Science 367, eaay4991. https://doi.org/10.1126/science.aay4991.

34. Goldie, B.J., and Cairns, M.J. (2012). Post-transcriptional trafficking and regulation of neuronal gene expression. Mol Neurobiol 45, 99-108. https://doi.org/10.1007/s12035-011-8222-0.

35. Beiki, H., Sturgill, D., Arango, D., Relier, S., Schiffers, S., and Oberdoerffer, S. (2024). Detection of ac4C in human mRNA is preserved upon data reassessment. Mol Cell 84, 1611-1625. e1613. https://doi.org/10.1016/j.molcel.2024.03.018.

36. Georgeson, J., and Schwartz, S. (2024). No evidence for ac4C within human

mRNA upon data reassessment. Mol Cell 84, 1601-1610. e1602. https://doi.org/10.1016/j.molcel.2024.03.017.

37. Li, B., Xi, W., Bai, Y., Liu, X., Zhang, Y., Li, L., Bian, L., Liu, C., Tang, Y., Shen, L., et al. (2023). FTO-dependent m(6)A modification of Plpp3 in circSCMH1-regulated vascular repair and functional recovery following stroke. Nat Commun 14, 489. https://doi.org/10.1038/s41467-023-36008-y.

38. Sinclair, W.R., Arango, D., Shrimp, J.H., Zengeya, T.T., Thomas, J.M., Montgomery, D.C., Fox, S.D., Andresson, T., Oberdoerffer, S., and Meier, J.L. (2017). Profiling cytidine acetylation with specific affinity and reactivity. ACS Chem Biol 12, 2922-2926. https://doi.org/10.1021/acschembio.7b00734.

39. Yu, F., Zhang, Y., Cheng, C., Wang, W., Zhou, Z., Rang, W., Yu, H., Wei, Y., Wu, Q., and Zhang, Y. (2020). Poly (A)-seq: A method for direct sequencing and analysis of the transcriptomic poly (A)-tails. PloS one 15, e0234696. https://doi.org/10.1371/journal.pone.0234696.

40. Vorhees, C.V., and Williams, M.T. (2006). Morris water maze: procedures for assessing spatial and related forms of learning and memory. Nat Protoc 1, 848-858. https://doi.org/10.1038/nprot.2006.116.

41. Hoz, L.d., Martin, S.J., and Morris, R.G.M. (2004). Forgetting, reminding, and remembering: the retrieval of lost spatial memory. PLoS Biol 2, e225. https://doi.org/10.1371/journal.pbio.0020225.

42. Zhang, W., Gao, J., Fan, L., Wang, J., He, B., Wang, Y., Zhang, X., and Mao, H. (2023). ac4C acetylation regulates mRNA stability and translation efficiency in osteosarcoma. Heliyon 9, e17103. https://doi.org/10.1016/j.heliyon.2023.e17103.

43. Cajigas, I.J., Tushev, G., Will, T.J., tom Dieck, S., Fuerst, N., and Schuman, E.M. (2012). The local transcriptome in the synaptic neuropil revealed by deep sequencing and high-resolution imaging. Neuron 74, 453-466. https://doi.org/10.1016/j.neuron.2012.02.036.

44. Hafner, A.S., Donlin Asp, P.G., Leitch, B., Herzog, E., and Schuman, E.M. (2019). Local protein synthesis is a ubiquitous feature of neuronal pre-and postsynaptic compartments. Science 364, eaau3644. https://doi.org/10.1126/science.aau3644.

45. Niu, M., Cao, W., Wang, Y., Zhu, Q., Luo, J., Wang, B., Zheng, H., Weitz, D.A., and Zong, C. (2023). Droplet-based transcriptome profiling of individual synapses. Nat Biotechnol 41, 1332-1344. https://doi.org/10.1038/s41587-022-01635-1.

46. Steward, O., Wallace, C.S., Lyford, G.L., and Worley, P.F. (1998). Synaptic activation causes the mRNA for the IEG Arc to localize selectively near activated postsynaptic sites on dendrites. Neuron 21, 741-751. https://doi.org/10.1016/s0896-6273(00)80591-7.

47. Lyford, G.L., Yamagata, K., Kaufmann, W.E., Barnes, C.A., Sanders, L.K., Copeland, N.G., Gilbert, D.J., Jenkins, N.A., Lanahan, A.A., and Worley, P.F. (1995). Arc, a growth factor and activity-regulated gene, encodes a novel cytoskeleton-associated protein that is enriched in neuronal dendrites. Neuron

14, 433-445. https://doi.org/10.1016/0896-6273(95)90299-6.
48. Das, S., Lituma, P.J., Castillo, P.E., and Singer, R.H. (2023). Maintenance of a short-lived protein required for long-term memory involves cycles of transcription and local translation. Neuron 111, 2051-2064 e2056. https://doi.org/10.1016/j.neuron.2023.04.005.
49. Steward, O., Farris, S., Pirbhoy, P.S., Darnell, J., and Driesche, S.J. (2014). Localization and local translation of Arc/Arg3.1 mRNA at synapses: some observations and paradoxes. Front Mol Neurosci 7, 101. https://doi.org/10.3389/fnmol.2014.00101.
50. Bramham, C.R., Alme, M.N., Bittins, M., Kuipers, S.D., Nair, R.R., Pai, B., Panja, D., Schubert, M., Soule, J., Tiron, A., and Wibrand, K. (2010). The Arc of synaptic memory. Exp Brain Res 200, 125-140. https://doi.org/10.1007/s00221-009-1959-2.
51. Yu, Q., Liu, Y.-Z., Zhu, Y.-B., Wang, Y.-Y., Li, Q., and Yin, D.-M. (2019). Genetic labeling reveals temporal and spatial expression pattern of D2 dopamine receptor in rat forebrain. Brain Struct Funct 224, 1035-1049. https://doi.org/10.1007/s00429-018-01824-2.
52. Madisen, L., Zwingman, T.A., Sunkin, S.M., Oh, S.W., Zariwala, H.A., Gu, H., Ng, L.L., Palmiter, R.D., Hawrylycz, M.J., and Jones, A.R. (2010). A robust and high-throughput Cre reporting and characterization system for the whole mouse brain. Nat Neurosci 13, 133-140. https://doi.org/10.1038/nn.2467.
53. Biane, J.S., Ladow, M.A., Stefanini, F., Boddu, S.P., Fan, A., Hassan, S., Dundar, N., Apodaca-Montano, D.L., Zhou, L.Z., and Fayner, V. (2023). Neural dynamics underlying associative learning in the dorsal and ventral hippocampus. Nat Neurosci 26, 798-809. https://doi.org/10.1038/s41593-023-01296-6.
54. Fanselow, M.S., and Dong, H.-W. (2010). Are the dorsal and ventral hippocampus functionally distinct structures? Neuron 65, 7-19. https://doi.org/10.1016/j.neuron.2009.11.031.
55. Moser, E., Moser, M.-B., and Andersen, P. (1993). Spatial learning impairment parallels the magnitude of dorsal hippocampal lesions, but is hardly present following ventral lesions. J Neurosci 13, 3916-3925. https://doi.org/10.1523/JNEUROSCI.13-09-03916.1993.
56. Lau, O.D., Courtney, A.D., Vassilev, A., Marzilli, L.A., Cotter, R.J., Nakatani, Y., and Cole, P.A. (2000). p300/CBP-associated factor histone acetyltransferase processing of a peptide substrate: kinetic analysis of the catalytic mechanism. J Biol Chem 275, 21953-21959. https://doi.org/10.1074/jbc.M003219200.
57. Shahi, K., and Baudry, M. (1993). Glycine-induced changes in synaptic efficacy in hippocampal slices involve changes in AMPA receptors. Brain Res 627, 261-266. https://doi.org/10.1016/0006-8993(93)90329-l.
58. Lu, W., Man, H., Ju, W., Trimble, W.S., MacDonald, J.F., and Wang, Y.T. (2001). Activation of synaptic NMDA receptors induces membrane insertion of new AMPA receptors and LTP in cultured hippocampal neurons. Neuron 29, 243-254. https://doi.org/10.1016/s0896-6273(01)00194-5.
59. Tsien, J.Z., Chen, D.F., Gerber, D., Tom, C., Mercer, E.H., Anderson, D.J.,

Mayford, M., Kandel, E.R., and Tonegawa, S. (1996). Subregion-and cell type–restricted gene knockout in mouse brain. Cell 87, 1317-1326. https://doi.org/10.1016/s0092-8674(00)81826-7.

60. Hedegaard, C., Kjaer-Sorensen, K., Madsen, L.B., Henriksen, C., Momeni, J., Bendixen, C., Oxvig, C., and Larsen, K. (2013). Porcine synapsin 1: SYN1 gene analysis and functional characterization of the promoter. FEBS Open Bio 3, 411-420. https://doi.org/10.1016/j.fob.2013.10.002.

61. Lv, J., Liu, H., Wang, Q., Tang, Z., Hou, L., and Zhang, B. (2003). Molecular cloning of a novel human gene encoding histone acetyltransferase-like protein involved in transcriptional activation of hTERT. Biochem Biophys Res Commun 311, 506-513. https://doi.org/10.1016/j.bbrc.2003.09.235.

62. Shen, Q., Zheng, X., McNutt, M.A., Guang, L., Sun, Y., Wang, J., Gong, Y., Hou, L., and Zhang, B. (2009). NAT10, a nucleolar protein, localizes to the midbody and regulates cytokinesis and acetylation of microtubules. Exp Cell Res 315, 1653-1667. https://doi.org/10.1016/j.yexcr.2009.03.007.

63. Saunders, A., Macosko, E.Z., Wysoker, A., Goldman, M., Krienen, F.M., de Rivera, H., Bien, E., Baum, M., Bortolin, L., Wang, S., et al. (2018). Molecular Diversity and Specializations among the Cells of the Adult Mouse Brain. Cell 174, 1015-1030 e1016. https://doi.org/10.1016/j.cell.2018.07.028.

64. Perea, G., Navarrete, M., and Araque, A. (2009). Tripartite synapses: astrocytes process and control synaptic information. Trends Neurosci 32, 421-431. https://doi.org/10.1016/j.tins.2009.05.001.

65. Eroglu, C., and Barres, B.A. (2010). Regulation of synaptic connectivity by glia. Nature 468, 223-231. https://doi.org/10.1038/nature09612.

66. Bramham, C.R., Worley, P.F., Moore, M.J., and Guzowski, J.F. (2008). The immediate early gene arc/arg3. 1: regulation, mechanisms, and function. Journal of Neuroscience 28, 11760-11767. https://doi.org/10.1093/nar/gkx1030.

67. Lisman, J., Yasuda, R., and Raghavachari, S. (2012). Mechanisms of CaMKII action in long-term potentiation. Nat Rev Neurosci 13, 169-182. https://doi.org/10.1038/nrn3192.

68. Tang, Y.P., Shimizu, E., Dube, G.R., Rampon, C., Kerchner, G.A., Zhuo, M., Liu, G., and Tsien, J.Z. (1999). Genetic enhancement of learning and memory in mice. Nature 401, 63-69. https://doi.org/10.1038/43432.

69. Tullis, J.E., Larsen, M.E., Rumian, N.L., Freund, R.K., Boxer, E.E., Brown, C.N., Coultrap, S.J., Schulman, H., Aoto, J., Dell'Acqua, M.L., and Bayer, K.U. (2023). LTP induction by structural rather than enzymatic functions of CaMKII. Nature 621, 146-153. https://doi.org/10.1038/s41586-023-06465-y.

70. Chen, X., Cai, Q., Zhou, J., Pleasure, S.J., Schulman, H., Zhang, M., and Nicoll, R.A. (2024). CaMKII autophosphorylation is the only enzymatic event required for synaptic memory. Proc Natl Acad Sci U S A 121, e2402783121. https://doi.org/10.1073/pnas.240278312.

71. Su, J., Huang, F., Tian, Y., Tian, R., Qianqian, G., Bello, S.T., Zeng, D., Jendrichovsky, P., Lau, C.G., and Xiong, W. (2023). Entorhinohippocampal cholecystokinin modulates spatial learning by facilitating neuroplasticity of

hippocampal CA3-CA1 synapses. Cell Rep 42, 113467. https://doi.org/10.1016/j.celrep.2023.113467.

72. Ji, H.-N., Zhou, H.-Q., Qie, J.-B., Lu, W.-M., Gao, H.-T., and Wu, D.-H. (2025). Dysregulated ac4C modification of mRNA in a mouse model of early-stage Alzheimer's disease. Cell & Bioscience 15, 45. https://doi.org/10.1186/s13578-025-01389-8.

73. Zhang, H.-L., Han, W., Du, Y.-Q., Zhao, B., Yang, P., and Yin, D.-M. (2021). SRC3 acetylates calmodulin in the mouse brain to regulate synaptic plasticity and fear learning. J Biol Chem 297, 101044. https://doi.org/10.1016/j.jbc.2021.101044.

74. Zhang, H.-L., Zhao, B., Han, W., Sun, Y.-B., Yang, P., Chen, Y., Ni, D., Zhang, J., and Yin, D.-M. (2021). Acetylation of calmodulin regulates synaptic plasticity and fear learning. J Biol Chem 297, 101034. https://doi.org/10.1016/j.jbc.2021.101034.

75. Zhang, H.-L., Zhao, B., Yang, P., Du, Y.-Q., Han, W., Xu, J., and Yin, D.-M. (2021). Steroid receptor coactivator 3 regulates synaptic plasticity and hippocampus-dependent memory. Neurosci Bull 37, 1645-1657. https://doi.org/10.1007/s12264-021-00741-5.

76. Zhang, H.L., Hu, S., Yang, P., Long, H.C., Ma, Q.H., Yin, D.M., and Xu, G.Y. (2024). HDAC9 - mediated calmodulin deacetylation induces memory impairment in Alzheimer's disease. CNS Neurosci Ther 30, e14573. https://doi.org/10.1111/cns.14573.

77. Drazic, A., Myklebust, L.M., Ree, R., and Arnesen, T. (2016). The world of protein acetylation. Biochim Biophys Acta 1864, 1372-1401. https://doi.org/10.1016/j.bbapap.2016.06.007.

78. Cui, Z., Xu, Y., Wu, P., Lu, Y., Tao, Y., Zhou, C., Cui, R., Li, J., and Han, R. (2023). NAT10 promotes osteogenic differentiation of periodontal ligament stem cells by regulating VEGFA-mediated PI3K/AKT signaling pathway through ac4C modification. Odontology 111, 870-882. https://doi.org/10.1007/s10266-023-00793-1.

79. Xu, C., Zhang, J., Zhang, J., and Liu, B. (2021). SIRT7 is a deacetylase of N4-acetylcytidine on ribosomal RNA. Genome Instab Dis 2, 253-260. https://doi.org/10.1007/s42764-021-00046-x.

80. Kudrin, P., Meierhofer, D., Vågbø, C.B., and Ørom, U.A.V. (2021). Nuclear RNA-acetylation can be erased by the deacetylase SIRT7. BioRxiv, 2021.2004.2006.438707. https://doi.org/10.1101/2021.04.06.438707.

81. Zhou, H.-Q., Zhuang, L.-J., Bao, H.-Q., Li, S.-J., Dai, F.-Y., Wang, P., Li, Q., and Yin, D.-M. (2022). Olfactory regulation by dopamine and DRD2 receptor in the nose. Proc Natl Acad Sci U S A 119, e2118570119. https://doi.org/10.1073/pnas.2118570119.

82. Rouillard, A.D., Gundersen, G.W., Fernandez, N.F., Wang, Z., Monteiro, C.D., McDermott, M.G., and Ma'ayan, A. (2016). The harmonizome: a collection of processed datasets gathered to serve and mine knowledge about genes and

proteins. Database (Oxford) 2016, 2016:baw2100. https://doi.org/10.1093/database/baw100.

83. Larrieu, D., Britton, S., Demir, M., Rodriguez, R., and Jackson, S.P. (2014). Chemical inhibition of NAT10 corrects defects of laminopathic cells. Science 344, 527-532. https://doi.org/10.1126/science.1252651.

84. Guo, X.-F., Wang, X.-H., Fu, Y.-L., Meng, Q., Huang, B.-Y., Yang, R., Guo, Y., Du, Y.-R., Wang, X., and Gao, Y. (2022). Elevation of N-acetyltransferase 10 in hippocampal neurons mediates depression-and anxiety-like behaviors. Brain Res Bull 185, 91-98. https://doi.org/10.1016/j.brainresbull.2022.05.004.

85. Hao, H., Liu, W., Miao, Y., Ma, L., Yu, B., Liu, L., Yang, C., Zhang, K., Chen, Z., Yang, J., et al. (2022). N4-acetylcytidine regulates the replication and pathogenicity of enterovirus 71. Nucleic Acids Res 50, 9339-9354. https://doi.org/10.1093/nar/gkac675.

86. Gao, S., Shen, R., Li, J., Jiang, Y., Sun, H., Wu, X., Li, X., Miao, C., He, M., Wang, J., and Chen, W. (2024). N-acetyltransferase 10 mediates cognitive dysfunction through the acetylation of GABABR1 mRNA in sepsis-associated encephalopathy. Proc Natl Acad Sci U S A 121, e2410564121. https://doi.org/10.1073/pnas.2410564121.

87. Plath, N., Ohana, O., Dammermann, B., Errington, M.L., Schmitz, D., Gross, C., Mao, X., Engelsberg, A., Mahlke, C., and Welzl, H. (2006). Arc/Arg3. 1 is essential for the consolidation of synaptic plasticity and memories. Neuron 52, 437-444. https://doi.org/10.1016/j.neuron.2006.08.024.

88. Chowdhury, S., Shepherd, J.D., Okuno, H., Lyford, G., Petralia, R.S., Plath, N., Kuhl, D., Huganir, R.L., and Worley, P.F. (2006). Arc/Arg3.1 interacts with the endocytic machinery to regulate AMPA receptor trafficking. Neuron 52, 445-459. https://doi.org/10.1016/j.neuron.2006.08.033.

89. Guzowski, J.F., Setlow, B., Wagner, E.K., and McGaugh, J.L. (2001). Experience-dependent gene expression in the rat hippocampus after spatial learning: a comparison of the immediate-early genesArc, c-fos, and zif268. Journal of Neuroscience 21, 5089-5098. https://doi.org/10.1523/JNEUROSCI.21-14-05089.2001.

90. Ting, A.K., Chen, Y., Wen, L., Yin, D.M., Shen, C., Tao, Y., Liu, X., Xiong, W.C., and Mei, L. (2011). Neuregulin 1 promotes excitatory synapse development and function in GABAergic interneurons. J Neurosci 31, 15-25. https://doi.org/10.1523/jneurosci.2538-10.2011.

91. Wu, D., Bacaj, T., Morishita, W., Goswami, D., Arendt, K.L., Xu, W., Chen, L., Malenka, R.C., and Südhof, T.C. (2017). Postsynaptic synaptotagmins mediate AMPA receptor exocytosis during LTP. Nature 544, 316-321. https://doi.org/10.1038/nature21720.

92. Thalalla Gamage, S., Sas-Chen, A., Schwartz, S., and Meier, J.L. (2021). Quantitative nucleotide resolution profiling of RNA cytidine acetylation by ac4C-seq. Nat Protoc 16, 2286-2307. https://doi.org/10.1038/s41596-021-00501-9.

93. Zhang, Y., Liu, T., Meyer, C.A., Eeckhoute, J., Johnson, D.S., Bernstein, B.E.,

Nusbaum, C., Myers, R.M., Brown, M., Li, W., and Liu, X.S. (2008). Model-based Analysis of ChIP-Seq (MACS). Genome Biol 9, R137. https://doi.org/10.1186/gb-2008-9-9-r137.

94. Heinz, S., Benner, C., Spann, N., Bertolino, E., Lin, Y.C., Laslo, P., Cheng, J.X., Murre, C., Singh, H., and Glass, C.K. (2010). Simple combinations of lineage-determining transcription factors prime cis-regulatory elements required for macrophage and B cell identities. Mol Cell 38, 576-589. https://doi.org/10.1016/j.molcel.2010.05.004.

95. Wu, T., Hu, E., Xu, S., Chen, M., Guo, P., Dai, Z., Feng, T., Zhou, L., Tang, W., and Zhan, L. (2021). clusterProfiler 4.0: A universal enrichment tool for interpreting omics data. Innovation (Camb) 2, 100141. https://doi.org/10.1016/j.xinn.2021.100141.

96. Guca, E., Alarcon, R., Palo, M.Z., Santos, L., Alonso-Gil, S., Davyt, M., de Lima, L.H., Boissier, F., Das, S., and Zagrovic, B. (2024). N6-methyladenosine in 5′ UTR does not promote translation initiation. Mol Cell 84, 584-595. e586. https://doi.org/10.1016/j.molcel.2023.12.028

97. Newman, A.M., Liu, C.L., Green, M.R., Gentles, A.J., Feng, W., Xu, Y., Hoang, C.D., Diehn, M., and Alizadeh, A.A. (2015). Robust enumeration of cell subsets from tissue expression profiles. Nat Methods 12, 453-457. https://doi.org/10.1038/nmeth.3337.

98. Tan, G.H., Liu, Y.Y., Hu, X.L., Yin, D.M., Mei, L., and Xiong, Z.Q. (2011). Neuregulin 1 represses limbic epileptogenesis through ErbB4 in parvalbumin-expressing interneurons. Nat Neurosci 15, 258-266. https://doi.org/10.1038/nn.3005.

99. Yin, D.-M., Chen, Y.-J., Lu, Y.-S., Bean, J.C., Sathyamurthy, A., Shen, C., Liu, X., Lin, T.W., Smith, C.A., and Xiong, W.-C. (2013). Reversal of behavioral deficits and synaptic dysfunction in mice overexpressing neuregulin 1. Neuron 78, 644-657. https://doi.org/10.1016/j.neuron.2013.03.028.

Methods

Animals

Male C57BL/6 mice were used throughout this study. For stereotaxic injection of AAV, six-week-old mice were used. For behavioral analysis, 9 to 10-week-old mice were used. For ac4C dot-blots, LC-MS/MS, acRIP-seq, mice aged between nine and ten weeks were used. For immunofluorescence, western blots and electrophysiology, ten-week-old mice were used. Animals were housed in rooms at 23°C and 50% humidity in a 12 h light/dark cycle and with food and water available ad libitum. Animal experimental procedures were approved by the Institutional Animal Care and Use Committee of East China Normal University. The Ai14 Cre-dependent tdTomato reporter mouse line (stock no. 007914) was obtained and used for generating reporter mice.

940 **Generation of Nat10$^{Cre/+}$ knockin mice**

941 The mouse Nat10 gene has 29 exons and the translational start codon (ATG) is localized
942 in exon 2. We employed CRISPR/Cas9 technology in conjunction with homologous
943 recombination to insert a Cre-WPRE-polyA expression cassette at the translational start
944 codon of the Nat10 gene in C57BL/6J mice. The process commenced with the synthesis
945 of Cas9 mRNA and a guide RNA (gRNA) targeting the start codon of Nat10, with the
946 gRNA sequence being 5′-catcatgaatcggaagaaggtgg-3′. A donor vector was then
947 constructed using In-Fusion cloning, containing 2.6 kb 5′ and 3′ homology arms
948 flanking the Cre-WPRE-pA cassette, designed for Cre recombinase expression,
949 enhanced by the WPRE element and concluded with a polyadenylation signal. The
950 cocktail of Cas9 mRNA, gRNA, and the donor vector was microinjected into fertilized
951 C57BL/6J mouse embryos, leading to the birth of F0 generation mice. These mice were
952 screened for the precise genomic integration of the cassette through PCR amplification
953 and sequencing. Successful modifications were observed in F0 mice, which were
954 subsequently bred with C57BL/6J mice to secure F1 progeny harboring the
955 modification.

956 The resulting offspring were genotyped using PCR, with primers designed to detect
957 the Cre within the Nat10 gene. The primers for genotyping wt Nat10 allele are as
958 follows: forward: 5’tgtctttcctgtggtggtgt3’; reverse: 5’tgcgcactgaaaccctacaa3’. the
959 primers for genotyping Nat10-cre allele are as follows: forward:
960 5’gaaatcatgcaggctggtgg3’; reverse: 5’aaagtcccggaaaggagctg3’. The PCR products for
961 wt Nat10 and Nat10-Cre alleles were 392 and 393 bp, respectively.

962 **Generation of Nat10$^{flox/flox}$ mice**

963 The generation of Nat10$^{flox/flox}$ mice involved targeted modification of exon 4 within
964 the Nat10 gene, utilizing CRISPR/Cas9-mediated gene editing. Two guide RNAs
965 (gRNAs) were specifically designed to target and flank exon 4, enabling a precise
966 floxed modification. The sequences for these gRNAs were as follows: gRNA1: 5′-
967 tcagcagaccactttaaagatgg-3′ and gRNA2: 5′-tgcctgacatagtaaggtctggg-3′. Both Cas9
968 mRNA and gRNAs were produced through in vitro transcription techniques. A donor
969 vector for homologous recombination was constructed using In-Fusion cloning. This
970 vector included a 3.0 kb 5′ homology arm, a 0.7 kb loxp-flanked region (flox), and a
971 3.0 kb 3′ homology arm to ensure accurate genomic insertion at the Nat10 locus. The
972 mixture of Cas9 mRNA and the two gRNAs was injected into the cytoplasm of one-

973 cell stage embryos. These embryos were subsequently implanted into pseudopregnant
974 females and carried to term. The resulting offspring were genotyped using PCR, with
975 primers designed to detect the floxed exon 4 of Nat10 gene. The primers for genotyping
976 the wt and floxed Nat10 allele are as follows: forward: 5'tgccgaggggatgtactcat3';
977 reverse: 5'agaaccccacgaactgtcct3'. The PCR products for wt Nat10 and floxed Nat10
978 allele were 302 and 356 bp, respectively.

979 **Morris water maze (MWM)**

980 The MWM, a widely recognized method for assessing spatial memory[40], was
981 implemented with the following protocol: mice were acclimated to the testing
982 environment over a period of three days through 10-minute daily handling sessions. To
983 aid navigation, visual cues were strategically positioned around the perimeter of the
984 maze. To ensure consistency and minimize the impact of external variables, all
985 experimental sessions were conducted simultaneously each day. During the core phase
986 of the experiment, spanning five days, mice were subjected to four trials daily. In each
987 trial, they were released from different quadrants into the maze, with the escape
988 platform being fixed in the first quadrant. A trial was deemed complete when a mouse
989 successfully located the platform within a 60-second timeframe. If unsuccessful, the
990 mouse was gently guided to the platform at the 60-second mark. The mice were handled
991 for 10 minutes each day following the completion of the four trials.

992 On Day 6, a probe test was conducted to assess memory retention: the platform
993 was removed, and mice were released from the third quadrant. The number of crossings
994 over the previous platform location during the 60-second trial was recorded. To
995 evaluate visual and motor function independent of spatial memory, a visible platform
996 test was conducted on a separate cohort of control mice. The platform was made visible
997 by placing a flag above the surface, and its location was changed between trials to
998 prevent spatial learning. Mice underwent four trials in one day, with performance
999 measured by latency to reach the visible platform. This design was chosen to match
1000 handling and navigation exposure, while minimizing spatial learning.

1001 On Day 20, a second probe test was conducted using the same conditions as on
1002 Day 6, to assess long-term memory retention after a two-week interval in the home cage.
1003 Control mice underwent both the visible platform test and were subjected to identical
1004 handling procedures and probe test conditions on Day 6 and Day 20. This design
1005 ensured that differences observed in probe test performance reflected spatial memory

1006 rather than sensory or motor deficits. Mice designated for molecular or histological
1007 analysis were euthanized 60 minutes after the probe test began. This time point was
1008 selected based on established literature indicating that memory retrieval-related
1009 molecular signatures, such as the activation of immediate early genes and RNA
1010 modifications, occur at this time[89].

1011 **Chemical and reagents**

1012 All chemicals and reagents utilized in this study were of analytical grade. RNA was
1013 extracted using TRIzol® Reagent (15596-026, Invitrogen, Carlsbad, CA, USA)
1014 following the manufacturer's protocol. Chloroform and other general laboratory
1015 chemicals were obtained from Merck (109634, Darmstadt, Germany). The ACQUITY
1016 HSS T3 column (2.1×100 mm, 1.8 μm) for LC-MS/MS analysis was purchased from
1017 Waters Corporation (186008499, Milford, MA, USA). Phosphodiesterase was obtained
1018 from Sigma (P3243-1VL, St. Louis, MO, USA). Nuclease P1 and alkaline phosphatase,
1019 used for RNA digestion, were obtained from Takara (2410A and 2250A).
1020 Hydroxylamine was from Aladdin Bio-Chem Technology Co., LTD (H164487). RNase
1021 inhibitor, which is critical for preserving RNA integrity during manipulations, was
1022 purchased from New England Biolabs (M0314S, NEB, CA, USA). Methylene blue,
1023 which is used for nucleic acid visualization, was obtained from Abcam (M9140). Poly-
1024 D-lysine was purchased from Sigma (Cat No. P1149). Tamoxifen was purchased from
1025 Sigma (Cat T5648).

1026 **Subcellular fractionation**

1027 The procedure of subcellular fractionation was adapted from the methodologies in our
1028 previous studies[73,74]. Mouse brain tissues were processed starting with homogenization
1029 in Buffer A, which consists of 0.32 M sucrose, 1 mM $MgCl_2$, 1 mM PMSF, and a
1030 protease inhibitor cocktail to ensure comprehensive cell lysis while preserving protein
1031 integrity. The resultant homogenates were then filtered to remove cell debris and
1032 subsequently subjected to centrifugation at 500g for 5 minutes using a fixed-angle rotor.
1033 This step separates the homogenate into the pellet (P1) and supernatant (S1) fractions.
1034 The P1 fraction, containing primarily nuclei and unbroken cells, was further purified
1035 by resuspension in Buffer B (10 mM KCl, 1.5 mM $MgCl_2$, and 10 mM Tris-HCl at pH
1036 7.4) followed by a repeat centrifugation under the same conditions to remove any
1037 remaining debris. The final pellet was resuspended in Buffer C (20 mM HEPES, pH
1038 7.9, 25% glycerol, 1.5 mM $MgCl_2$, 1.4 M KCl, 0.2 mM EDTA, 0.2 mM PMSF, and 0.5

1039 mM DTT), which is designed for nuclear protein extraction and incubated with
1040 agitation at 4 °C for 30 minutes to facilitate the release of nuclear proteins. A final
1041 centrifugation at 12,000g for 10 minutes was performed, and the supernatant,
1042 containing the nuclear protein fraction, was collected. The initial supernatant (S1),
1043 following the removal of P1, was further centrifuged at 10,000g for 10 minutes to
1044 partition it into the P2 fraction, which included the crude synaptosomes, and the
1045 cytosolic S2 fraction.

1046 **Western blot**

1047 Homogenates of hippocampus tissue were prepared in the RIPA buffer containing 50
1048 mM Tris-HCl, pH 7.4, 150 mM NaCl, 2 mM EDTA, 1% sodium deoxycholate, 1%
1049 SDS, 1 mM PMSF, 50 mM sodium fluoride, 1 mM sodium vanadate, 1 mM DTT, and
1050 protease inhibitors cocktails. All the protein samples were boiled at 100 °C water bath
1051 for 10 minutes before western blot. Homogenates were resolved on SDS/PAGE and
1052 then transferred to nitrocellulose membranes, which were incubated in the TBS buffer
1053 (0.1% Tween-20 and 5% milk) for 1 hour at room temperature followed by incubation
1054 of primary antibodies overnight at 4 °C. After washing, the membranes were incubated
1055 with HRP-conjugated secondary antibody in the same TBS buffer for 2 hours at room
1056 temperature. Immunoreactive bands were visualized by ChemiDocTM XRS + Imaging
1057 System (BIO-RAD) using enhanced chemiluminescence (Pierce) and analyzed with
1058 Image J (NIH). The following primary antibodies were used: anti-Histone H3 (1:1000,
1059 Cell Signaling, 9715), anti-SYN1 (1:1000, Cell Signaling, 2312), anti-α-tubulin
1060 (1:10000, Cell Signaling, 3873), anti-NAT10 (1:1000, Abcam, ab194297), anti-Acetyl-
1061 Histone H3 (1:1000, Cell Signaling, 9649), anti-ARC (1:1000, Proteintech, 66550-1-
1062 Ig), anti-PSD95 (1:1000, Cell Signaling, 3450), anti-PCAF (1:1000, Cell Signaling,
1063 3378), and anti-GAPDH (1:5000, Abways, ab0037). The following secondary
1064 antibodies were used: HRP-conjugated secondary antibody (goat-anti-mouse, G-21040;
1065 goat-anti-rabbit, G-21234; 1:2000, Thermo Fisher).

1066 **Immunofluorescence**

1067 The mouse brains were fixed in 4% paraformaldehyde at room temperature for 1 hour
1068 and dehydrated in 20% sucrose at 4 ℃ overnight. Then the tissues were placed in an
1069 embedding mold and frozen in OCT media at 0 ℃. The embedded tissues were cut into
1070 slices with the thickness of 30 μm using a Leica microtome (CM3050S). The brain
1071 slices were permeabilized with 0.3% Triton-X 100 and 5% BSA in PBS and incubated

with primary antibodies at 4 °C overnight. After washing with PBS for three times, samples were incubated with secondary antibodies for 2 hours at room temperature. Samples were mounted with Vectashield mounting medium (Vector Labs) and images were taken by Leica TCS SP8 confocal microscope. The following primary antibodies were used: rabbit anti-NeuN (1:1000, Abcam, ab177487), rabbit anti-Neurogranin (1:500, Abcam, ab217672). The following secondary antibodies were employed: Rabbit IgG (H+L) Highly Cross-Adsorbed Secondary Antibody (A32732, 1:500, Thermo Fisher). Unbiased stereology TissueFAX Plus ST (Tissue Gnostics, Vienna, Austria) was applied to count the number of Nat10-positive neurons. The detailed methods for cell number counting are available on the website (https://tissuegnostics.com/products/single-cell-analysis/tissuequest).

Detection of ac4C and m6A modifications by LC-MS/MS

1 μg of total RNA or polyA RNA was digested by 4 μl of nuclease P1 in 40 μl buffer (10 mM Tris-HCl, pH 7.0, 100 mM NaCl, 2.5 mM $ZnCl_2$) at 37°C for 12 hours, followed by incubation with 1 μl of alkaline phosphatase at 37°C for 2 hours. The RNA solution was then diluted to 100 μl and analyzed by LC-MS/MS. The separation of nucleosides was accomplished by means of an Agilent C18 column, and detection was achieved by AB SCIEX QTRAP 5500. Standard curves were generated to reflect the linear relationship between the ac4C (or C) concentration and their peak area during the LC-MS/MS analysis. A known concentration of ac4C or C that falls into the linear range of the standard curve (i.e, the standard samples) was analyzed alongside with the testing samples. The concentration of ac4C or C in the testing samples were calculated through normalization of the peak areas from testing samples by that from standard samples. The stoichiometry levels of ac4C were determined by the ratio of concentration of ac4C to C. The same strategies were used for analysis of the stoichiometry levels of m6A.

ac4C and m6A dot-blot

The total RNA of mouse hippocampus was extracted with Trizol according to the manufacturer's instructions. The polyA RNA was then purified using the Dynabeads™ polyA RNA purification kit (61006, Thermo Fisher). The dot-blot was performed according to the previous study[27]. We used 0.5 μg of polyA RNA that fall in the linear range for each blot. For each HOM replicate, we purified 0.5 μg of polyA RNA from the hippocampus of one mouse. In contrast, for each SYN replicate, we purified 0.5 μg

of polyA RNA from the hippocampus of five mice. In brief, the polyA RNA was denatured at 95 °C for 5 min using a heat block, immediately kept on ice for 1 min, loaded onto Amersham Hybond-N+ membrane and crosslinked with UV254 for 30 min. The membranes were blocked with 5% nonfat milk for 2 h at room temperature (RT), and incubated with the rabbit anti-m6A (1:2000, Synaptic System, #202003) or anti-ac4C antibody (1:500, Abcam, ab252215) at 4°C overnight. After wash with 0.05% PBST for three times, the membranes were incubated with the HRP-conjugated secondary antibody (goat-anti-rabbit, G-21234, 1:2000, Thermo Fisher) at RT for 2 h. The signals were visualized by ChemiDocTM XRS + Imaging System (BIO-RAD) using ECL and analyzed with Image J (NIH). RNA loading was verified by staining the membranes with 0.2% methylene blue. The intensity of each dot was normalized to total RNA.

Primary neuronal culture

The primary culture of mouse hippocampal neurons was performed according to our previous studies[90]. Hippocampal explants from embryonic day 16 (E16) mouse embryos were digested with 0.125% trypsin solution for 30 min at 37°C, followed by trituration with pipette in plating medium (DMEM with 10% fetal bovine serum, 10% F-12, and 1% penicillin-streptomycin). The dissociated neurons were plated onto poly-D-lysine-coated coverslips at a density of 1×10^5 cells per 35 mm dish. Following a 4-hour incubation period, the plating medium was replaced with Neurobasal™ medium (Thermo Fisher, 21103049) supplemented with 2% B-27™ (Thermo Fisher, 17504044), 1% GlutaMax™ (Thermo Fisher, 35050061), and 1% penicillin-streptomycin (Invitrogen). Cytarabine (Sigma, C1768-100MG) was added after 2 days to a final concentration of 1 μM, to inhibit the proliferation of dividing non-neuronal cells. Half volume of the culture medium was replaced every 3-4 days with freshly prepared medium. The neurons were harvested at 14 days in vitro (DIV 14) for immunofluorescence experiments.

Chemical LTP (cLTP) and immunofluorescence

For cLTP, neurons were incubated with 300 μM glycine in a cell incubator set at 37°C with 5% CO_2 and 95% humidity for 3 minutes, followed by an additional 60 minutes without glycine at 37°C [91]. Neurons were then fixed with 4% paraformaldehyde for 30 minutes on ice to preserve cell membranes. After washing with PBS, the neurons were penetrated with 0.3% Triton-X100 and blocked with 1% BSA in PBS for 30 min at RT.

1138 After that, neurons were incubated with primary antibodies (chicken anti-MAP2
1139 antibody, 1:2000, Abcam, ab5392; mouse monoclonal anti-PSD95 antibody, 1:800,
1140 Abcam, ab192757; and rabbit monoclonal anti-NAT10 antibody, 1:800, Abcam,
1141 ab194297) overnight at 4°C. Neurons were then washed by PBS for three times before
1142 incubation with fluorescent secondary antibodies for 2 hours at 37°C. The following
1143 secondary antibodies were employed: Chicken IgY (H+L) Secondary Antibody (A-
1144 11039, 1:500, Thermo Fisher), Rabbit IgG (H+L) Cross-Adsorbed Secondary Antibody
1145 (A-21244, 1:500, Thermo Fisher), Rabbit IgG (H+L) Highly Cross-Adsorbed
1146 Secondary Antibody (A32732, 1:500, Thermo Fisher), and Mouse IgG (H+L) Highly
1147 Cross-Adsorbed Secondary Antibody (A32727, 1:500, Thermo Fisher). After washing
1148 with PBS, the neurons were placed on mounting solution with DAPI (Beyotime, P0131).
1149 Confocal stacks were acquired from 3-6 individual fields on multiple coverslips per
1150 culture using a Leica SP8 confocal microscope. Two independent cultures were
1151 analyzed for each condition, including vehicle-treated control and glycine-treated
1152 neurons.

1153 **Regular acRIP-seq for HOM**

1154 The acRIP-seq was performed following the previous studies[19,92]. The total RNA was
1155 extracted from the HOM of mouse hippocampus using TRIzol, the quality of the RNA
1156 was evaluated through gel electrophoresis in order to ascertain its integrity and purity,
1157 and the concentration and purity of the RNA were detected. Total RNA samples,
1158 initially 100 μg, were treated with the rRNA depletion kit (New England Biolabs, Cat.
1159 No. E6310) to remove rRNA. After rRNA depletion, the RNA was subjected to
1160 immunoprecipitation using the anti-ac4C antibodies and the ac4C RIP kit (GenSeq, Cat
1161 No. GS-ET-005) according to the manufacturer's instructions. Briefly, total RNAs were
1162 randomly fragmented to ~200 nt by RNA Fragmentation Reagents (NEB, Cat No.
1163 M0348S). Protein A/G Dynabeads (Share-Bio, SB-PR001) were coupled to the anti-
1164 ac4C antibody by rotating at room temperature for 1 h. The RNA fragments were then
1165 incubated with the beads-linked anti-ac4C antibodies (2 μg) in the 100 μl acRIP buffer
1166 (PBS containing 1% Triton X-100, 2 mM BSA, and 1 mM RNase inhibitor) and rotated
1167 at 4°C for 4 h. After incubation, the RNA/antibody complexes were washed for four
1168 times with the acRIP buffer, and then RNAs were eluted by elution buffer (containing
1169 0.1 M Glycine, 0.5% Triton X-100, PH 2.5-3.1) at room temperature for 10 minutes.
1170 Finally, add NaOH solution to adjust the pH of the elution product to neutral. Both the

1171 immunoprecipitated RNA and 1% input RNA are reverse transcribed with random
1172 hexamers, followed by RNA library preparation with Ultra™ II Directional RNA
1173 Library Prep Kit (New England Biolabs, Cat No. E7760) according to the
1174 manufacturer's instructions.

1175 The quality of RNA libraries was assessed using Agilent 2100 bioanalyzer and then
1176 subjected to the next-generation sequencing through the NovaSeq 6000 platform
1177 (Illumina). The quality of the sequencing data is measured using Q30 scores, and low-
1178 quality reads and 3' adaptors are removed using Cutadapt (v1.9.3). High-quality reads
1179 are then aligned to the reference genome using Hisat2 (v2.0.4). Raw counts are
1180 generated using HTSeq (v0.9.1) and normalized using edgeR (v3.16.5). Gene
1181 expression was quantified by logged transcript per million mapped reads (log_2TPM)
1182 (with a cutoff TPM >1). The ac4C peaks and mRNAs that were identified from at least
1183 two of the three biological replicates of HOM were considered reliable.

1184 **Low-input acRIP-seq for SYN**

1185 The low-input acRIP-seq included some modifications, compared with the regular
1186 acRIP-seq. First, the RNA amount is relatively smaller (~ 2 μg, purified from the
1187 hippocampus of 10 mice) for low-input acRIP-seq, compared with regular acRIP-seq
1188 (~ 100 μg, purified from the hippocampus of 2 mice). Second, the total RNA purified
1189 from the SYN was not treated by the rRNA depletion kit before acRIP to avoid the non-
1190 specific RNA loss during the rRNA depletion process. Third, the RNA libraries for low-
1191 input acRIP-seq were generated by a different kit - SMARTer Stranded Total RNA-Seq
1192 Kit v2-Pico Input Mammalian (Takara, Cat No. 634413). To increase the data reliability
1193 for low-input acRIP-seq, transcripts that were identified in our own sequencing and at
1194 least two of the three synaptosome databases[43-45] were considered reliable and included
1195 in the analysis. Considering the principle of 3Rs (replacement, reduction and refinement)
1196 for animal ethics, we used one biological replicate for each time point from control and
1197 learning mice, but each replicate consists of SYN RNA purified from 10 mice. The
1198 mitochondrially encoded mRNAs and long non-coding RNA (lncRNA) were filtered
1199 out before analysis of the acRIP-seq data since the current study focused on ac4C of
1200 regular mRNA in the SYN.

1201 **Identification of ac4C peaks**

1202 Following RNA integrity assessments, acRIP enrichment verification, and library
1203 quality checks, raw sequencing reads from both acRIP and input samples underwent

rigorous quality control. Initially, sequencing quality was evaluated using Q30 scores and FastQC to ensure base-level accuracy. Low-quality reads and 3' adaptor sequences were identified and removed using Cutadapt software (v1.9.3), resulting in high-quality clean reads for further analysis.

Post-alignment filtering was applied to exclude reads that mapped to mitochondrial DNA (chrM) and non-concordant mate pairs, which often arise from sequencing artifacts or alignment errors. The remaining clean reads were then aligned to the mouse genome (mm10) using Hisat2 software (v2.0.4), with parameters allowing a maximum of five mismatches per read to ensure alignment accuracy above 95%. Ensembl gene annotations (Release 75) were incorporated to guide accurate mapping to annotated regions. To account for transcript variability, canonical transcript sequences from the UCSC genome browser were used to generate a Bowtie2 index, enabling transcriptome mapping. Reads were aligned in local mode, which is well-suited for fragmented RNA sequences.

Acetylation peaks (ac4C peaks) were identified using MACS software (v1.4.2)[93], optimized for transcriptomic data. The shifting model and local lambda options were disabled to accommodate the unique characteristics of transcriptome data, and the genome size was set according to the total transcript base count. Input samples were used as controls to distinguish true ac4C-enriched peaks from background noise. The fold enrichment (FE) of ac4C peak was calculated though the MACS software by normalizing the read counts of acRIP ac4C peak to that of input ac4C peak. We established strict screening criteria in the peak calling process: adjusted $P < 0.05$ and $FE > 2$. The adjusted p-value was acquired by MACS software using a Poisson distribution model after posthoc Benjamini-Hochberg analysis. The ac4C peaks were generated on the UCSC genome browser (https://genome.ucsc.edu/cgi-bin/hgGateway) using the IGV software (http://www.igv.org/).

Sequence motif analysis

Sequence motifs were identified using HOMER[94] and visualized using ggseqlogo package from R software. HOMER identifies motifs that are specifically enriched on learning set of sequences relative to control (e.g., peaks upstream and downstream sequences relative to the entire genome sequence) based primarily on the principle of ZOOPS scoring with hypergeometric enrichment.

Gene ontology and functional category analysis

Gene ontology (GO) analysis to detect enrichment for GO terms in differential acetylation genes in R using the clusterProfiler[95], and the possible roles of these differential acetylation genes were annotated according to MF, BP and CC. GO terms with a false-discovery rate adjusted P.adj of < 0.05 were visualized using R scripts to plot. The R package clusterProfiler to visualize the genes composing KEGG pathways, and P.adj < 0.05 was used as the threshold of significant enrichment.

Analysis of ac4C fold enrichment (FE) for individual mRNA

The FE of ac4C mRNA was reflected by the average FE values of all ac4C peaks identified in the entire transcript including the 5'UTR, CDS and 3'UTR. Averaging the cumulative distribution of these peaks offers a more comprehensive overview of the abundance of ac4C modifications across the mRNA molecule, avoiding the artificial increase of FE of long mRNAs[96]. Additionally, in instances where ac4C modifications on mRNA are more dispersed or present in low abundance, a single prominent peak may not be observable; instead, multiple low-abundance peaks might emerge. In such scenarios, the accumulation of multiple peaks can enhance detection sensitivity, better capture dynamic changes, and mitigate biases inherent in individual experiments.

$$Average\ FE\ of\ ac4C = \frac{\Sigma peak\ (1 + 2 + 3 \ldots\ldots + n)}{n}$$

Analysis of ac4C fold change (FC) for individual mRNA

The fold change of ac4C mRNA is representative of the degree of change in the overall acetylation level of mRNA in the learning group (L) compared with the control group (C). To prevent a value of 0 in the denominator in the FC calculation, we added 1 to the FE of ac4C. The FC of ac4C mRNA was calculated using the following quantification index:

$$FC\ of\ ac4C = \frac{(FE\ of\ ac4C + 1)\ in\ L}{(FE\ of\ ac4C + 1)\ in\ C}$$

Analysis of PPI network

The STRING (https://string-db.org/) (version 12.0) knowledge base was used to create a protein-protein interaction (PPI) network. The PPI network was generated with a confidence score of 0.7 and visualized using Cytoscape (version 3.10.1). Molecular Complex Detection (MCODE) (v2.0.3) algorithm was employed to identify the components of the densely connected network.

1269 **The following software and algorithms were used for the quantification and**
1270 **statistical analysis of ac4C epitranscriptome.**

Software and algorithms, application, authors		
R v4.3.2	Statistical computing and graphics.	R Core Team. R Foundation for Statistical Computing 2023.
Python v3.11	Object-oriented programming language.	Van R et al. CreateSpace 2009.
ggplot2	Creating graphics, based on The Grammar of Graphics.	Hadley W et al, Springer-Verlag New York 2016.
ggseqlogo	Generating publication-ready sequence logos using ggplot2.	Wagih et al. Bioinformatics 2018.
tidyverse	Collection of R packages designed for data science.	Wickham et al. Journal of Open Source Software 2019.
ComplexHeat map	Arrange multiple heatmaps and supports annotation graphics.	Gu Z et al. Bioinformatics 2016.
HOMER v4.11	Motif Discovery and gene sequencing analysis.	Heinz S et al. Mol Cell 2010.
bedtools	Compare large sets of genomic features.	Aaron Q et al. Bioinformatics 2010.
cutadapt v1.9.3	Remove sequencing data adaptor.	Martin M. EMBnet 2011.
Hisat2 v2.04	Mapping sequencing reads to a single reference genome.	Zhang Y et al. Genome Research 2021.
MACS v1.4.2	Identifying transcript factor binding sites.	Yong Z et al. Genome Biology 2008.
Pandas v2.1.4	Cleaning data.	The pandas development team. Zenodo 2020.
IGV	Interactive genome visualization application.	James T et al. Bioinformatics 2023.
HTSeq (v0.9.1)	Analysing high-throughput sequencing data.	Simon A et al. Bioinformatics 2014.
edgeR (v3.16.5)	Empirical analysis of digital gene expression data.	McCarthy DJ et al. Nucleic Acids Research 2012.
CIBERSORT	Cell-type identification by	Aaron M et al. Nature methods

	estimating relative subsets of RNA transcripts.	2015.

Identification of relative abundance of genes in different cell types

We applied the CIBERSORT (Cell-type Identification by Estimating Relative Subsets of RNA Transcripts) algorithm[97] in R to determine the enriched cell types where the genes of NASA mRNAs were expressed. To construct the reference gene signature matrices, we used Dataset C from McCarroll Lab (http://dropviz.org/)[63] to extract gene expression features for various hippocampal cell types, including excitatory neurons, inhibitory neurons, astrocytes, and microglia. These reference matrices were then used to deconvolve the gene expression data and estimate the contributions from each cell type.

RT-qPCR

The cDNA was obtained through reverse transcription using the HiScript III RT SuperMix for qPCR kit (Vazyme, R323-01), followed by amplification using the ChamQ Universal SYBR qPCR Master Mix kit (Vazyme, Q711-02). Gene expression levels measured with RT-PCR were normalized to Gapdh. The primers used in qPCR for this study were as follows: Gapdh-forward, 5'gggtgtgaaccacgagaaat3'; Gapdh-reverse 5'actgtggtcatgagcccttc3'; Arc-forward, 5'ggagggaggtcttctaccgtc3'; Arc-reverse 5'cccccacacctacagagaca3'; Grin2b-forward, 5'ctggtgaccaatggcaagcatg3'; Grin2b-reverse, 5'ggcacagagaagtcaaccacct3'; Camk2α-forward, 5'agccatcctcaccactatgctg3'; Camk2α-reverse 5'gtgtcttcgtcctcaatggtgg3'.

Stereotaxic injection of AAV into mouse hippocampus

AAV2/9-Syn1-EGFP and AAV2/9-Syn1-EGFP-P2A-Cre were generated by Hanbio Technology (Shanghai) Corp., Ltd., with a titer of 10^{12}/μl. We injected 0.3 μl AAV into each side of the mouse hippocampus. Six-week-old $Nat10^{flox/flox}$ mice received an intraperitoneal injection of alphaxalone at a dosage of 40 mg/kg for anesthesia and then were immobilized in a stereotaxic frame provided by RWD Life Science. Similarly, AAV2/9-CAG-DIO-EGFP, generated by Hanbio Technology (Shanghai) Corp., Ltd., with a titer of 10^{12}/μl, was injected into the hippocampus of seven-week-old $Nat10^{Cre/+}$ and $ALDH1L1^{Cre/ERT2}$ mice. The AAVs were delivered into mouse hippocampus through a stereotaxic injector at a flow rate of 0.1 μl/min. The precise coordinates for the stereotaxic injection were set to anteroposterior (AP) −2.3 mm, dorsoventral (DV)

−1.8 mm, and mediolateral (ML)±1.75 mm, relative to the Bregma. To induce Cre enzyme expression, mice were fed a custom-made tamoxifen-infused diet over a period of one week[98].

Electrophysiological recording

Hippocampal slices were prepared as previously described[99]. Briefly, mice (10 weeks old, male) were decapitated and transverse hippocampal slices (400 μm) were prepared using a Vibroslice (VT 1000S; Leica) in ice-cold ACSF. For field potential recording, the same ACSF was used for slice preparation and recording: 120 mM NaCl, 2.5 mM KCl, 1.2 mM NaH_2PO_4, 2.0 mM $CaCl_2$, 2.0 mM $MgSO_4$, 26 mM $NaHCO_3$ and 10 mM glucose. After sectioning, hippocampal slices were allowed to recover in the chamber for 30 min at 34°C and then for a further 2-8 h at room temperature (25 ± 1°C). All solutions were saturated with 95% O_2/5% CO_2 (vol/vol).

The slices were placed in the recording chamber, which was superfused (3 mL/min) with ACSF at 32-34°C. fEPSPs were evoked in the CA1 stratum radiatum by stimulating the SC with a bipolar stimulating electrode (FHC) and recorded in current clamp using a HEKA EPC 10 amplifier (HEKA Elektronik) with ACSF-filled glass pipettes (1-3 MΩ). Test stimuli consisted of monophasic 100-μs pulses of constant current (intensity adjusted to produce 25% of the maximum response) at a frequency of 0.033 Hz. The strength of synaptic transmission was determined by measuring the initial amplitude of fEPSPs. L-LTP was induced by 4 trains of 100 Hz stimuli of 50 pulses each at 100 Hz, 10 s apart, at the same intensity as the test stimulus. The level of E-LTP / L-LTP was determined at an average of 55-60 / 115-120 min after HFS stimulation. To study glutamatergic transmission at SC-CA1 synapses, we recorded fEPSP input/output (I/O) curves at SC-CA1 synapses. To construct an I/O curve, fEPSPs were evoked by a series of incremental intensities (0.02-0.2 mA in 0.02 mA increments, 100 μs duration, at 0.033 Hz). Whole-cell patch-clamp recordings from CA1 neurons were visualized with infrared optics using an upright microscope equipped with a 40× water-immersion objective (BX51WI; Olympus) and an infrared-sensitive CCD camera. To analyze the intrinsic excitability of CA1 pyramidal neurons, the current clamp was used and neurons were held at 0 pA and then injected with step

currents (duration: 500 ms; increments: 20 pA; range: -100 to 400 pA; interval: 10 s). The input-output relationship was determined by plotting the injected currents against the number of action potentials. All data were acquired at a sampling rate of 10 kHz using PATCHMASTER version 2 x 90.1 software (HEKA Elektronik) and filtered off-line at 1 kHz.

Generation and use of the ac4C website

The ac4Catlas website was constructed using HTML (a scripting language for front-end development), PHP (a scripting language for backend development), and MySQL (a structured query language for data operation). All the website codes were deployed in a Linux server equipped with Centos environment. The raw data, processed data and annotated files were stored in "Data Downloads" section. JBrowse (https://jbrowse.org) was integrated to visualize the ac4C epitranscriptomic data on genomic regions of interest. Briefly, ac4Catlas provides user-friendly interactive interfaces which allow researchers to freely browse and perform extended operations, such as searching, comparing, and downloading. Besides, the browse module stores detailed information of samples and corresponding datasets as well as ac4C levels of mRNA and differentially acetylated regions between groups.

Statistical analysis

The cumulative distribution curve was analyzed by Kolmogorov-Smirnov test in R. The statistical analysis of percentage of ac4C summits occurring within CDS or UTRs was performed by chi-square test in R. The regular quantification data were shown as mean ± SEM unless otherwise mentioned. The sample size justification was based on the previous studies and met the requirement of statistics power. For normally distributed data with 1 experimental variable, statistical analyses were performed by parametric analysis: unpaired (two-tailed) student's t-test for two groups and one-way ANOVA with the Tukey's multiple-comparison test for 3 groups. Data with >1 experimental variable were evaluated by two-way ANOVA, with post hoc Tukey, Dunnett or Sidak's multiple-comparison tests. All these statistical analyses were performed by the software of GraphPad Prism 10. Statistically significant difference was indicated as follows: ***

$P < 0.001$, ** $P < 0.01$ and * $P < 0.05$.

Acknowledgements

We thank CloudSeq Inc. (Shanghai, China) for providing us with technical support on acRIP-seq. This work was supported by STI2030-Major Projects (Grant No. 2021ZD0202500), Pudong New Area Science and Technology Development Foundation of Shanghai, China (Grant No. PKJ2022-Y34), Natural Science Foundation of Chongqing, China (Grant No. 2022NSCQ-MSX5813), and the Proton Cluster Incubation Project of the National Natural Science Foundation of China (Grant No. 2025GZRFY01).

Author contributions

H.-Q.Z. and H.J. performed biochemical and behavioral analysis, H.-Q.Z., Z.Z. and J.-W.Z. analyzed the data, W.-P.L., Y.-Y.D., and S.L. performed electrophysiology. D.-M.Y. conceived the idea, supervised the work and wrote the paper. All authors approved the final version of the manuscript.

Competing interests

The authors declare no competing interests.

Data and materials availability

All data are available in the main text, supplementary or source data files. The original data of acRIP-seq is accessible via the website (http://ac4Catlas.com/) or GEO database (GSE261922). All unique materials used are readily available from the corresponding author upon reasonable requests.

Code availability

Custom code used in this paper is available at https://github.com/YinDMlab/ac4CRIP-seq-analysis.

Figures and Legends

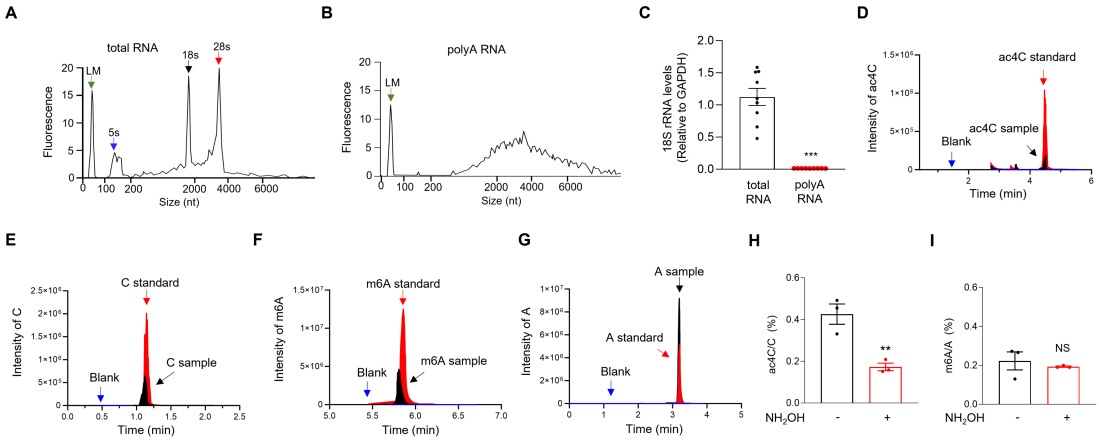

Figure 1 The presence of ac4C modification in PolyA RNA of mouse hippocampus. (A, B) Verification of the purity of PolyA RNA through the bioanalyzer profiling. The x-axis represents the size of nucleotides, and the y-axis represents the fluorescent signal from the bioanalyzer. LM, Lower Marker. (A), total RNA. (B), PolyA RNA. (C) Diminished levels of 18S rRNA in the polyA RNA samples, compared with total RNA samples, which was revealed by RT-qPCR analysis. The levels of 18S rRNA were normalized by that of Gapdh. *** $P < 0.0001$, two-tailed t-test, $n = 6$ biological replicates. (D-G) The chromatograms of blank, standard and testing samples of ac4C (D), C (E), m6A (F) and A (G) in the LC-MS/MS analysis. Shown are the representative peaks of ac4C, C, m6A and A identified in the polyA RNA samples purified from the HOM of mouse hippocampus. (H) Reduction of ac4C levels by the chemical deacetylation protocol. The stoichiometry levels of ac4C in polyA RNA from control and NH_2OH-treated samples were quantified. ** $P = 0.008$, two-tailed t-test, $n = 3$ biological replicates. (I) Unchanged m6A levels by the chemical deacetylation protocol. The stoichiometry levels of m6A in polyA RNA from control and NH_2OH-treated samples were quantified. NS, not significant, two-tailed t-test, $n = 3$ biological replicates. Quantification data are expressed as mean ± SEM.

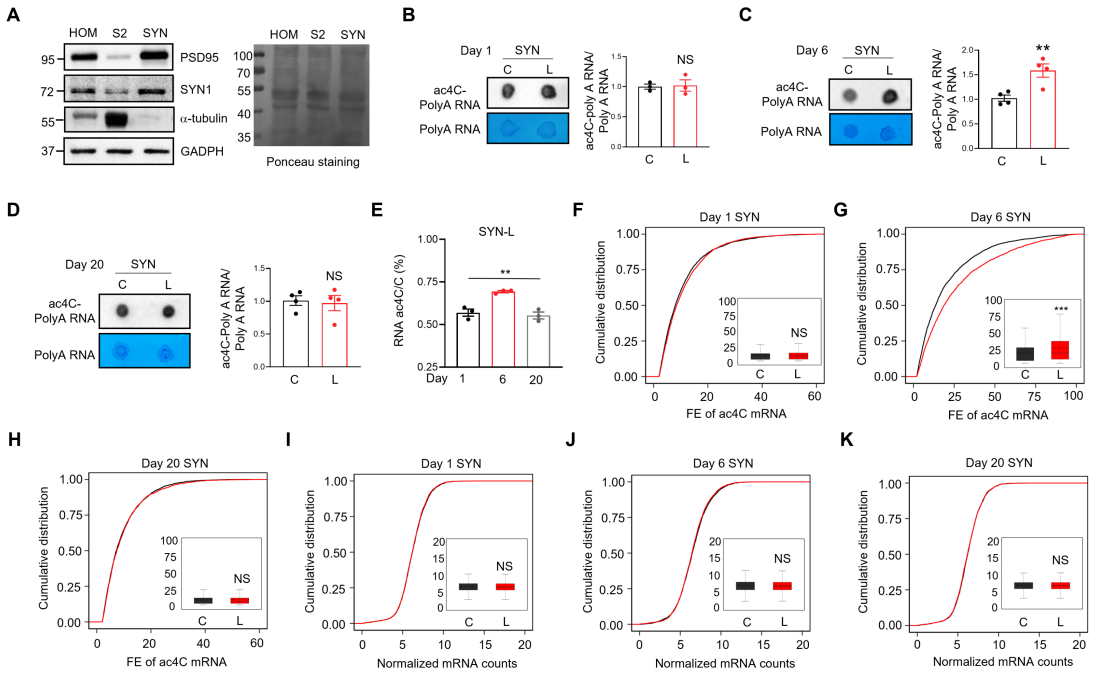

Figure 2 Increased mRNA acetylation in the SYN of mouse hippocampus after memory. (A) The purified synaptosomes (SYN) of mouse hippocampus expressed high levels of PSD95 and synapsin 1 (SYN1), two synaptic protein markers, but very low levels of α-tubulin, a cytoplasmic protein marker. The homogenates (HOM), cytoplasm (S2) and SYN of mouse hippocampus were subjected to western blots with the indicated antibodies. Left panel, representative images of western blots; right panel, Ponceau staining to show equal protein loading. (B) Acetylation of polyA RNA was not altered in SYN of mouse hippocampus at day 1. The polyA RNA purified from the SYN of control and learning mice at day 1 after MWM training were subjected to ac4C dot-blots and methylene blue staining. Left, the representative images; right, quantification data. NS, not significant, two-tailed t-test, n = 3 biological replicates. Data were normalized by controls. (C) Acetylation of polyA RNA was increased in the SYN of mouse hippocampus at day 6. The polyA RNA purified from the SYN of control and learning mice at day 6 after MWM training were subjected to ac4C dot-blots and methylene blue staining. Left, the representative images; right, quantification data. ** P = 0.0093, two-tailed t-test, n = 4 biological replicates. Data were normalized by controls. (D) Acetylation of polyA RNA was not altered in the SYN of mouse hippocampus at day 20. The polyA RNA purified from the SYN of control and learning

mice at day 20 after MWM training were subjected to ac4C dot-blots and methylene blue staining. Left, the representative images; right, quantification data. NS, not significant, two-tailed t-test, n = 4 biological replicates. Data were normalized by controls. (E) Acetylation of RNA in the SYN was increased during memory but returned to normal levels after forgetting. The stoichiometry levels of ac4C of total RNA purified from the SYN of learning (L) mice were shown at days 1, 6 and 20 after MWM training. ** P = 0.0023, one-way-ANOVA, n = 3 biological replicates. (F-H) Acetylation of mRNA was increased after memory but returned to normal levels after forgetting in the SYN of mouse hippocampus. Shown are cumulative distribution curves of FE of ac4C mRNA purified from the SYN of control (C) and learning (L) mice at days 1 (F), 6 (G), and 20 (H) after MWM training. The FE of ac4C mRNA was quantified in the quartile boxplots, where the solid line in the box is the median and the dashed line is the mean, where the maximum and minimum values are identified. NS, not significant, *** adj-P = 9.9814e-13, Kolmogorov-Smirnov test. (I-K) The total mRNA levels were not significantly altered in the SYN of mouse hippocampus during memory. Shown are cumulative distribution curves of normalized mRNA counts for SYN in control (C) and learning (L) mice at days 1 (I), 6 (J) and 20 (K) after MWM training. The normalized mRNA counts were quantified in the quartile boxplots, where the solid line in the box is the median and the dashed line is the mean, where the maximum and minimum values are identified. NS, not significant, Kolmogorov-Smirnov test. C, control; L, learning. FE, Fold Enrichment. Quantification data are expressed as mean ± SEM.

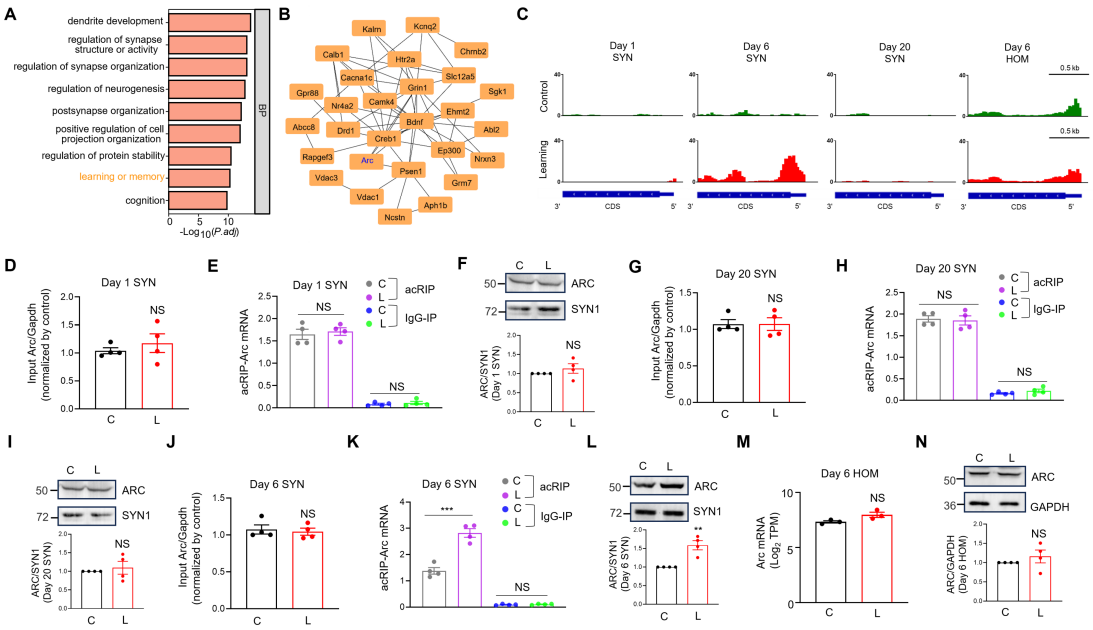

Figure 3 A representative MISA mRNA for Arc. (A) The biological processes (BP) in which MISA mRNAs are significantly overrepresented. The x-axis represents the negative logarithm of the adjusted p-value, reflecting the significance of the enrichment, while the y-axis shows the biological processes. (B) The protein-protein interaction (PPI) network of MISA mRNA implicated in the BP of learning or memory. P < 1.0e-16, Hypergeometric Test**.** (C) Increased ac4C modification of Arc in the SYN rather than in the HOM at day 6. Also note the unaltered ac4C Arc mRNA at days 1 or 20 in the SYN. Shown are the IGV maps of the ac4C peaks from the 3' UTR to the 5' UTR of Arc mRNA. The ac4C peaks were represented by acRIP/input (See details in the Method). (D, G) Arc mRNA levels from the input of SYN were not altered at days 1 (D) or 20 (G) after MWM training. The RNA purified from the SYN was subjected to the RT-qPCR analysis. NS, not significant, two-tailed t-test, n = 4 biological replicates. The levels of Arc mRNA were normalized by that of Gapdh in each sample, and then the ratio of Arc to Gapdh were normalized by controls. (E and H) The ac4C modification of Arc mRNA was not altered in the SYN at days 1 (E) or 20 (H) after MWM training. The RNA purified through the acRIP and IgG-IP products of SYN was subjected to the RT-qPCR analysis. NS, not significant, two-way-ANOVA followed by Tukey's multiple comparison test, n = 4 biological replicates. Data were normalized by input. (F and I**)** The protein levels of ARC did not change in the SYN at days 1 (F) or

20 (I) after MWM training. Top, representative western blot images; bottom, quantification data. NS, not significant, two-tailed t-test, n = 4 biological replicates. The protein levels of ARC were normalized by that of SYN1 in each sample, and then the ratio of ARC to SYN1 were normalized by controls. (J) Arc mRNA levels from the input of SYN were not altered at day 6 after MWM training. The RNA purified from the SYN was subjected to the RT-qPCR analysis. NS, not significant, two-tailed t-test, n = 4 biological replicates. The levels of Arc mRNA were normalized by that of Gapdh in each sample, and then the ratio of Arc to Gapdh were normalized by controls. (K) The ac4C modification of Arc mRNA was significantly increased in the SYN at day 6 after MWM training. The RNA purified from the acRIP and IgG-IP products of SYN was subjected to the RT-qPCR analysis. *** $P < 0.001$, two-way-ANOVA followed by Tukey's multiple comparison test, n = 4 biological replicates. Data were normalized by input. (L) The protein levels of ARC were significantly increased in the SYN at day 6 after MWM training. Top, representative western blot images; bottom, quantification data. ** $P = 0.0032$, two-tailed t-test, n = 4 biological replicates. The protein levels of ARC were normalized by that of SYN1 in each sample, and then the ratio of ARC to SYN1 were normalized by controls. (M) Arc mRNA levels from the HOM were not altered at day 6 after MWM training. The Arc mRNA levels were revealed by the $\log_2$TPM from the next-generation sequencing of the HOM RNA. NS, not significant, two-tailed t-test, n = 3 biological replicates. (N) The protein levels of ARC did not change in the HOM at day 6 after MWM training. Top, representative western blot images; bottom, quantification data. NS, not significant, two-tailed t-test, n = 4 biological replicates. The protein levels of ARC were normalized by that of GAPDH in each sample, and then the ratio of ARC to GAPDH were normalized by controls. C, control; L, learning. Quantification data are expressed as mean ± SEM.

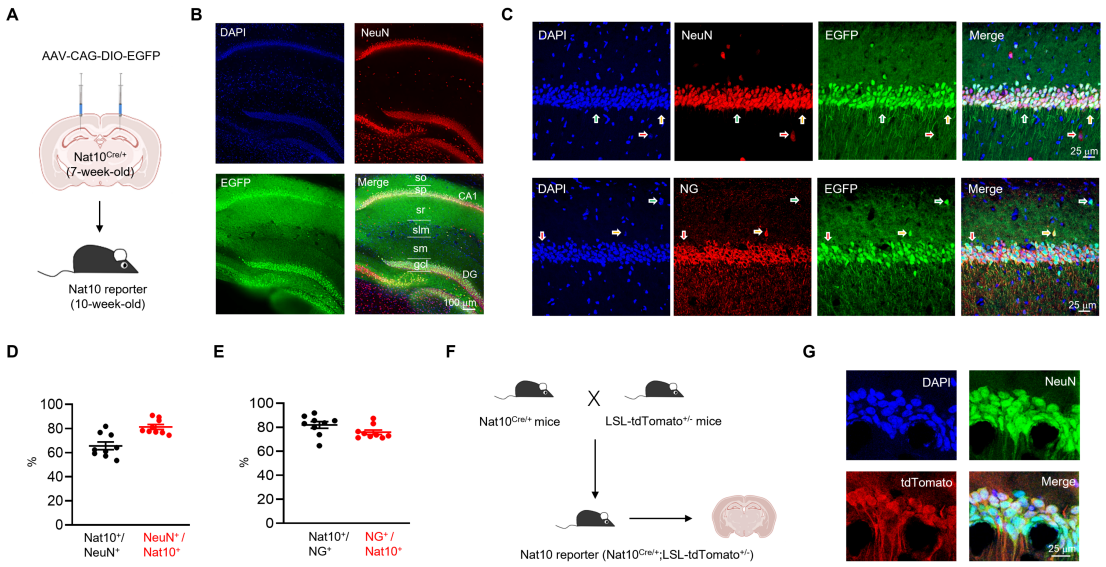

Figure 4 Expression of Nat10 in mature neurons of mouse hippocampus. (A) Experimental design. Cre-reporting AAV was injected into the dorsal hippocampus of 7-week-old Nat10$^{Cre/+}$ mice. Three weeks after AAV injection, the fluorescent protein EGFP was analyzed in the Nat10 reporter mice. (B) Co-localization of EGFP with NeuN in the hippocampus of Nat10 reporter mice. The hippocampal slices from Nat10 reporter mice were immunostained with anti-NeuN antibodies. so, stratum oriens; sp, stratum pyramidale; sr, stratum radiatum; slm, stratum lacunosum-moleculare; sm, stratum moleculare; gcl, granule cell layer; DG: dentate gyrus. Scale bar, 100 μm. (C) Co-localization of EGFP and NeuN or NG in the CA1 region of Nat10 reporter mice. The hippocampal slices from Nat10 reporter mice were immunostained with anti-NeuN or anti-NG antibodies. The yellow arrow indicates a neuron or excitatory pyramidal neuron that expresses Nat10, whereas the red arrow represents a neuron or excitatory pyramidal neuron that does not express Nat10. The green arrow indicates a non-neuronal cell that expresses Nat10. Scale bar, 25 μm. (D) Quantification of the percentage of NeuN-positive cells expressing Nat10 (Nat10^{+} / NeuN^{+} = 65.61 ± 3.245%) and the percentage of Nat10-positive cells expressing NeuN (NeuN^{+} / Nat10^{+} = 81.31 ± 2.029%). n = 9 slices from 3 mice. (E) Quantification of the percentage of NG-positive cells expressing Nat10 (Nat10^{+} / NG^{+} = 81.87 ± 2.765%) and the percentage of Nat10-positive cells expressing NG (NG^{+} / Nat10^{+} = 75.82 ± 1.882%). n = 9 slices from 3 mice. (F) Experimental design of generate Nat10 reporter mice. (G) Co-localization

of tdTomato with NeuN in the hippocampus of Nat10 reporter mice. The hippocampal slices from Nat10 reporter mice were immunostained with anti-NeuN antibodies. Scale bar, 25 μm.

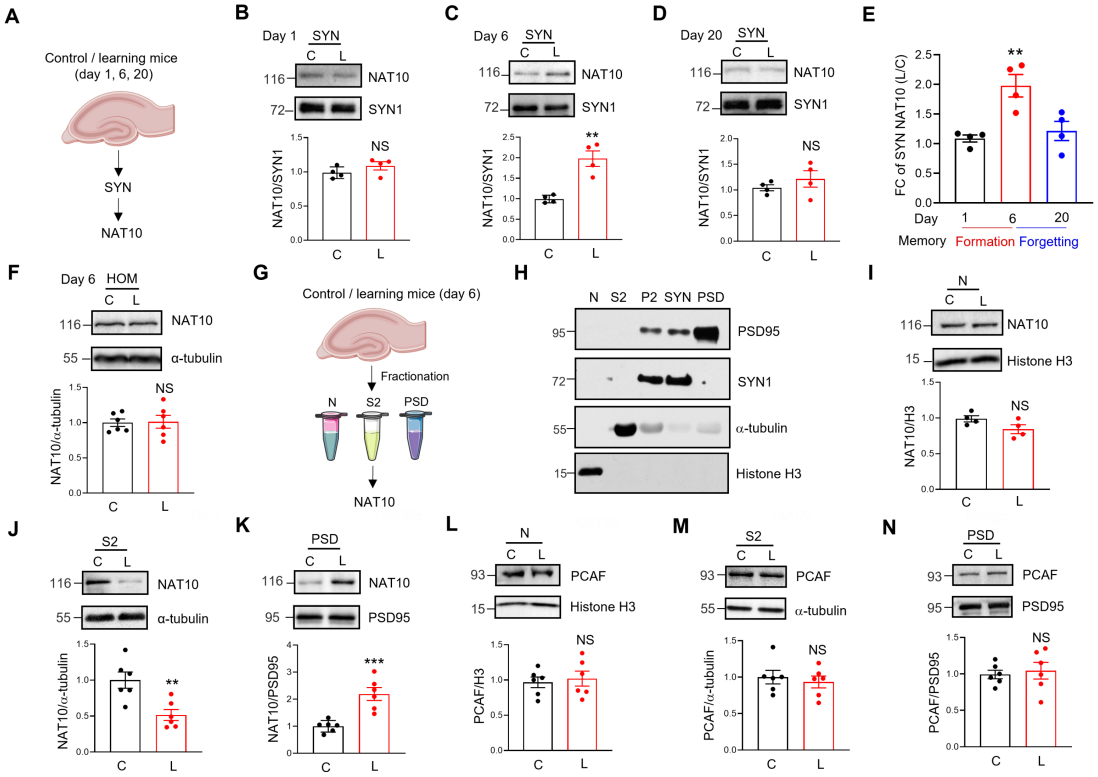

Figure 5 Increased NAT10 proteins in the SYN of mouse hippocampus after memory. (A) Experimental design. The SYN fractions were purified from the hippocampus of control and learning mice at days 1, 6 and 20. The NAT10 protein levels in the SYN were then assessed by western blots. (B-D) Protein levels of NAT10 were increased in the SYN after memory but returned to normal levels after forgetting. The SYN proteins from control and learning mice at days 1 (B), 6 (C), and 20 (D) were subjected to western blots with the indicated antibodies. The protein levels of NAT10 were normalized by that of SYN1 in each sample, and then the ratio of NAT10 to SYN1 was normalized by controls. Top, representative western blot images; bottom, quantification data. NS, not significant, ** P = 0.0023, two-tailed t-test, n = 4 biological replicates. (E) The fold change (FC) of NAT10 proteins in panel (B-D) was quantified. ** P = 0.0043, one-way-ANOVA, n = 4 biological replicates. (F) Protein levels of NAT10 were not altered in the HOM at day 6. The HOM proteins from control and

learning mice at day 6 were subjected to western blots with the indicated antibodies. Top, representative western blot images; bottom, quantification data. NS, not significant, two-tailed t-test. Data were normalized by controls, n = 6 biological replicates at each condition. The protein levels of NAT10 were normalized by that of α-tubulin in each sample, and then the ratio of NAT10 to α-tubulin was normalized by controls. (G) Experimental design. Proteins were extracted from nucleus (N), cytoplasm (S2), and postsynaptic density (PSD) of control and learning mouse hippocampus at day 6, and then NAT10 protein levels were assessed by western blots. (H) Expression of different protein markers in the nuclear (N), cytoplasmic (S2), P2 (Crude synaptosomes fraction), SYN, and PSD fractions of mouse hippocampus. Shown are representative images of western blots. Protein samples purified from different subcellular fractions of mouse hippocampus were subjected to western blots with the indicated antibodies. (I) Protein levels of NAT10 were not altered in the nuclear fraction of mouse hippocampus after memory. The nuclear protein samples from control and learning mice at day 6 were subjected to western blots with the indicated antibodies. Top, representative western blot images; bottom, quantification data. NS, not significant, two-tailed t-test, n = 4 biological replicates. The protein levels of NAT10 were normalized by that of Histone H3 proteins in each sample, and then the ratio of NAT10 to Histone H3 was normalized by controls. (J) Protein levels of NAT10 were significantly reduced in the S2 fraction of mouse hippocampus after memory. The cytoplasmic protein samples from control and learning mice at day 6 were subjected to western blots with the indicated antibodies. Top, representative western blot images; bottom, quantification data. ** P = 0.0052, two-tailed t-test, n = 6 biological replicates. The protein levels of NAT10 were normalized by that of α-tubulin in each sample, and then the ratio of NAT10 to α-tubulin was normalized by controls. (K) Protein levels of NAT10 were significantly increased in the PSD fraction of mouse hippocampus after memory. The PSD protein samples from control and learning mice at day 6 were subjected to western blots with the indicated antibodies. Top, representative western blot images; bottom, quantification data. *** P = 0.0008, two-tailed t-test. n = 6 biological replicates. The

protein levels of NAT10 were normalized by that of PSD95 in each sample, and then the ratio of NAT10 to PSD95 was normalized by controls. (L-N) Protein levels of PCAF were not altered in the nuclear (L), S2 (M), or PSD fraction (N) of mouse hippocampus after memory. The protein samples purified from the different subcellular fractions of the hippocampus of control and learning mice at day 6 were subjected to western blots with the indicated antibodies. Top, representative western blot images; bottom, quantification data. NS, not significant, two-tailed t-test, n = 6 biological replicates. The protein levels were normalized by the protein markers in different subcellular fractions and then were normalized by controls. C, control; L, learning. Quantification data are expressed as mean ± SEM.

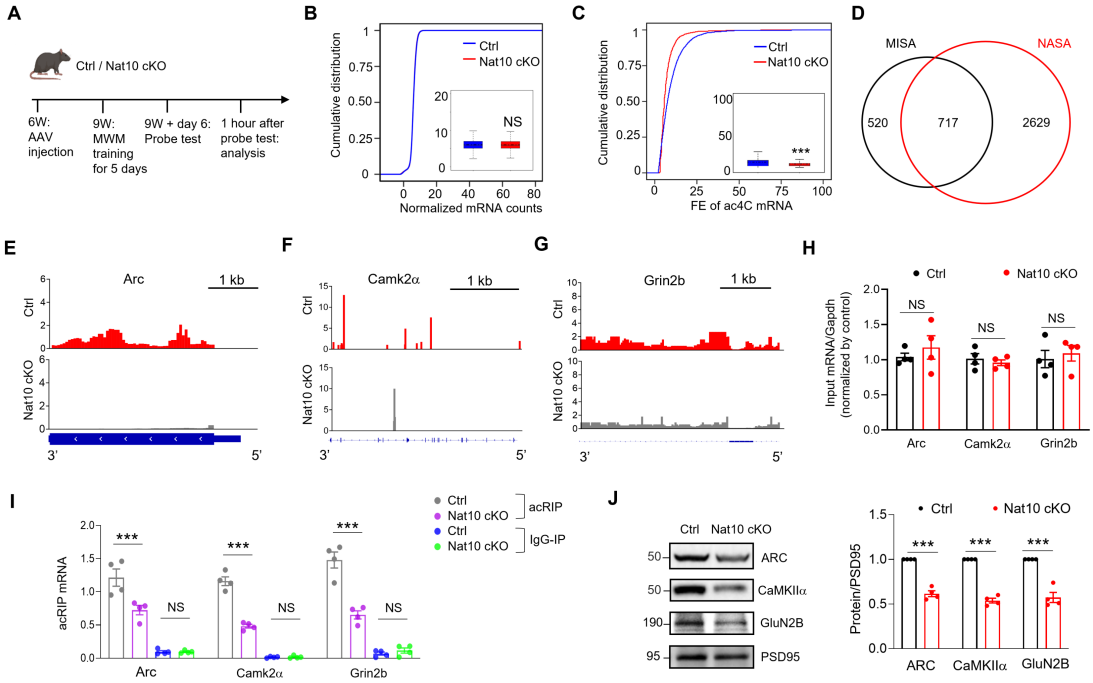

Figure 6 NAT10-dependent of ac4C modification of memory-related mRNAs in the SYN of learning mice. (A) Experimental design. Three weeks after AAV injection, the control (Ctrl) and Nat10 conditional knockout (cKO) mice were subjected to MWM training and probe test, and then the SYN fractions were purified from hippocampal tissues for low-input acRIP-seq. (B) The total mRNA levels were not significantly altered in the SYN of Nat10 cKO mice, compared to controls. Shown are cumulative distribution curves of normalized mRNA counts for SYN in control and Nat10 cKO

mice at day 6 after MWM training. The normalized mRNA counts were quantified in the quartile boxplots, where the solid line in the box is the median and the dashed line is the mean, where the maximum and minimum values are identified. NS, not significant, Kolmogorov-Smirnov test. (C) Acetylation of mRNA in the SYN of Nat10 cKO mice was significantly reduced, compared with controls. Shown are cumulative distribution curves of FE of ac4C mRNA purified from the SYN of control and Nat10 cKO mice at day 6 after MWM training. The FE of ac4C mRNA was quantified in the quartile boxplots, where the solid line in the box is the median and the dashed line is the mean, where the maximum and minimum values are identified. *** adj-P = 1.20076e-12, Kolmogorov-Smirnov test. (D) Venn diagrams show overlapping between MISA mRNA and NASA mRNA. (E-G) Reduced ac4C modification of Arc (E), Camk2α (F), and Grin2b (G) mRNA in the SYN of Nat10 cKO mice at day 6, compared with controls. Shown are the IGV maps of the ac4C peaks from the 3' UTR to the 5' UTR of transcripts. The ac4C peaks were represented by acRIP/input (See details in the Method). (H) The mRNA levels of Arc, Camk2α and Grin2b from the input of SYN were similar between control and Nat10 cKO mice. The RNA purified from the SYN was subjected to the RT-qPCR analysis. NS, not significant, two-tailed t-test, n = 4 biological replicates. The levels of mRNA were normalized by that of Gapdh in each sample, and then the ratio of mRNA to Gapdh were normalized by controls. (I) The ac4C modification of Arc, Camk2α, and Grin2b mRNA was significantly reduced in the SYN of Nat10 cKO mice at day 6, compared with controls. The RNA purified from the acRIP and IgG-IP products of SYN was subjected to the RT-qPCR analysis. *** P < 0.001, two-way-ANOVA followed by Tukey's multiple comparison test, n = 4 biological replicates. Data were normalized by input. (J) The protein levels of ARC, CaMKIIα and GluN2B were significantly increased in the SYN of Nat10 cKO mice at day 6, compared with controls. Left, representative western blot images; right, quantification data. *** P < 0.001, two-tailed t-test, n = 4 biological replicates. The protein levels were normalized by that of PSD95 in each sample, and then the ratio of protein to PSD95 were normalized by controls. Quantification data are expressed as

mean ± SEM.

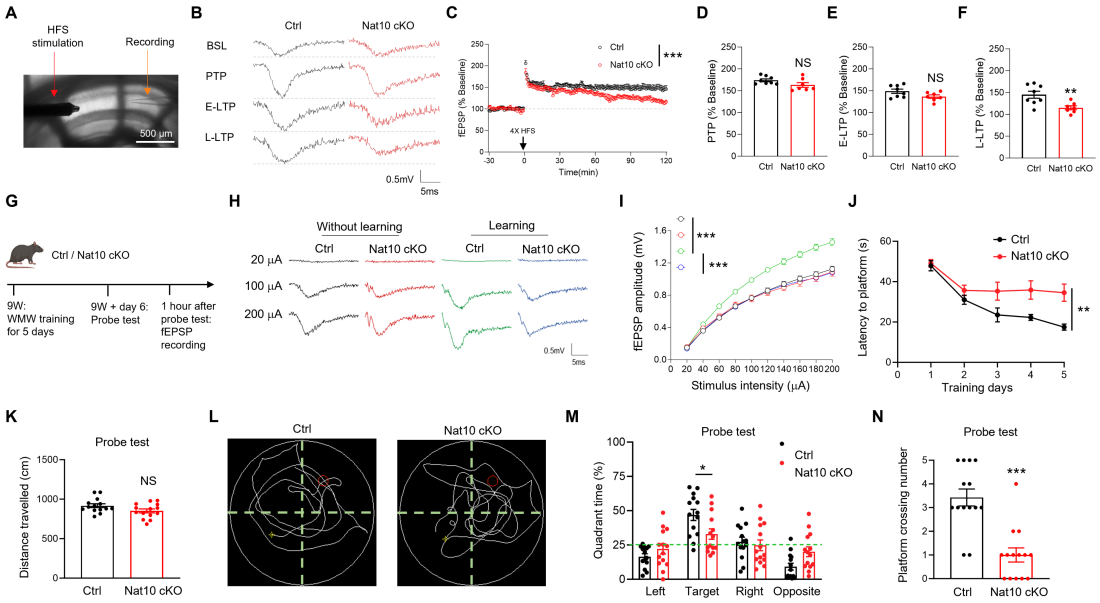

Figure 7 Impaired LTP as well as memory in the Nat10 cKO mice. (A) A representative image showing recording LTP at the SC-CA1 synapses from Nat10 cKO mice using the protocol of high-frequency stimulation (HFS). Scale bar, 500 μm. (B) The representative fEPSP traces from baseline (BSL), post-tetanus potentiation (PTP), early phase of LTP (E-LTP, 55-60 min after HFS) and late phase of LTP (L-LTP, 115-120 min after HFS). (C) Impaired maintenance of L-LTP at the SC-CA1 synapses in Nat10 cKO mice, compared with controls. Normalized fEPSP amplitudes were plotted every 1 min for hippocampal slices from control and Nat10 cKO mice. *** $P < 0.001$, two-way ANOVA, n = 8 slices from 4 mice for each group. (D) Normal LTP induction at the SC-CA1 synapses in Nat10 cKO mice, compared to controls. The PTP in panel C was quantified. NS, not significant, two-tailed t-test. n = 8 slices from 4 mice for each group. (E) Unaltered E-LTP at the SC-CA1 synapses in Nat10 cKO mice, compared to controls. The E-LTP in panel **c** was quantified. NS, not significant, two-tailed t-test. n = 8 slices from 4 mice for each group. (F) Impaired L-LTP at the SC-CA1 synapses in Nat10 cKO mice, compared with controls. The L-LTP in panel **c** was quantified. ** $P = 0.008$, two-tailed t-test. n = 8 slices from 4 mice for each group. (G) Experimental design. The control and Nat10 cKO mice were subjected to fEPSP recording at the SC-

CA1 synapses after training and probe test in the MWM. (H, I) Memory-induced enhancement of glutamatergic transmission at SC-CA1 synapses was significantly impaired in Nat10 cKO mice, compared with controls. (H) Representative fEPSP traces from control and Nat10 cKO mice. (I) Quantification of the fEPSP amplitudes in panel (H). *** Genotype $F_{(3, 680)} = 128.2$, $P < 0.001$, two-way ANOVA followed by Sidak's multiple comparison test, n = 18 slices from 5 mice each group. (J) Impaired learning process in Nat10 cKO mice, compared with controls. Shown are the learning curves of control and Nat10 cKO mice in the MWM. n = 14 mice per group, ** Genotype $F_{(1, 130)} = 24.08$, ** $P = 0.0014$, two-way ANOVA followed by Sidak's multiple comparison test. (K) Similar distance travelled during probe tests between control and Nat10 cKO mice. NS, not significant, two-tailed t-test, n = 14 mice per group. (L) Representative swimming traces of control and Nat10 cKO mice during probe tests. (M) Time spent in the target quadrant was significant reduced in Nat10 cKO groups during probe tests, compared with controls. * $P = 0.0198$, two-way ANOVA followed by Sidak's multiple comparison with post hoc t-test, n = 14 mice per group. (N) Number of platform crossing was significantly reduced in Nat10 cKO mice during probe tests, compared with controls. *** $P < 0.001$, two-tailed t-test, n = 14 mice per group. Quantification data are expressed as mean ± SEM.

Supplementary Figures

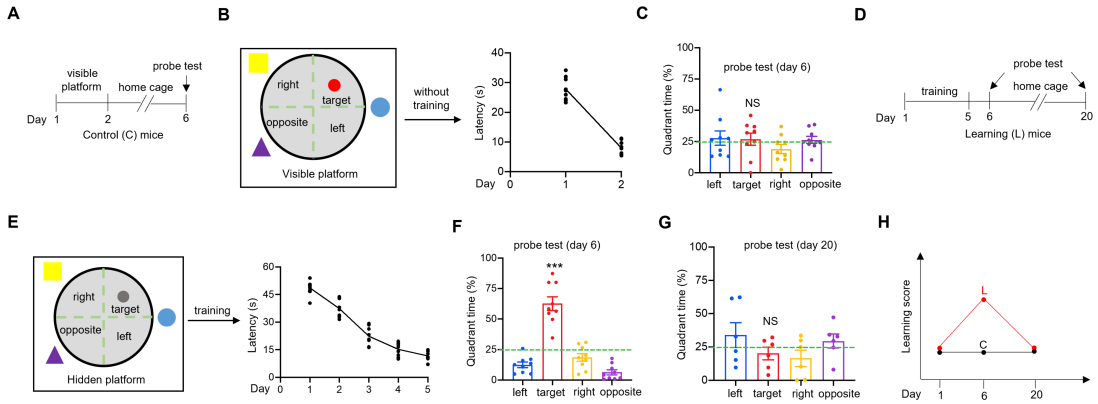

Supplementary Figure 1 Protocols of MWM for control and learning mice. (A) MWM protocol for control mice. The control mice were placed in MWM with a visible

platform at day 1 and 2, after which they returned to home cage and were subjected to probe tests at day 6. (B) Control mice were able to discern the visible platform above the water surface and consequently locate it rapidly. Shown are the latency to find the visible platform at day 1 and 2. (C) Control mice were not able to remember the target quadrant during probe tests on day 6. Shown are the percentage of time staying in each quadrant during probe tests. n = 9 mice, NS, not significant, one-way ANOVA. (D) MWM protocol for learning mice. The learning mice were trained in MWM with a hidden platform from day 1 to 5, and then were subjected to probe tests at day 6 and 20. (E) Learning mice showed improvement in their ability to find the hidden platform during the training process. Shown are the learning curves. (F) Learning mice could remember the target quadrant during probe tests at day 6. Shown are the percentage of time staying in each quadrant during probe tests. n = 9 mice, *** P < 0.001, one-way ANOVA. (G) Learning mice could not remember the target quadrant during probe tests at day 20. Shown are the percentage of time staying in each quadrant during probe tests. n = 6 mice, NS, not significant, one-way ANOVA. (H) Schematic summary of learning score of control and learning mice at day 1, 6, and 20 after MWM training. Memories were recalled at day 6 but were forgotten at day 20 in learning mice. The learning score indicates spatial memory performance in the MWM test.

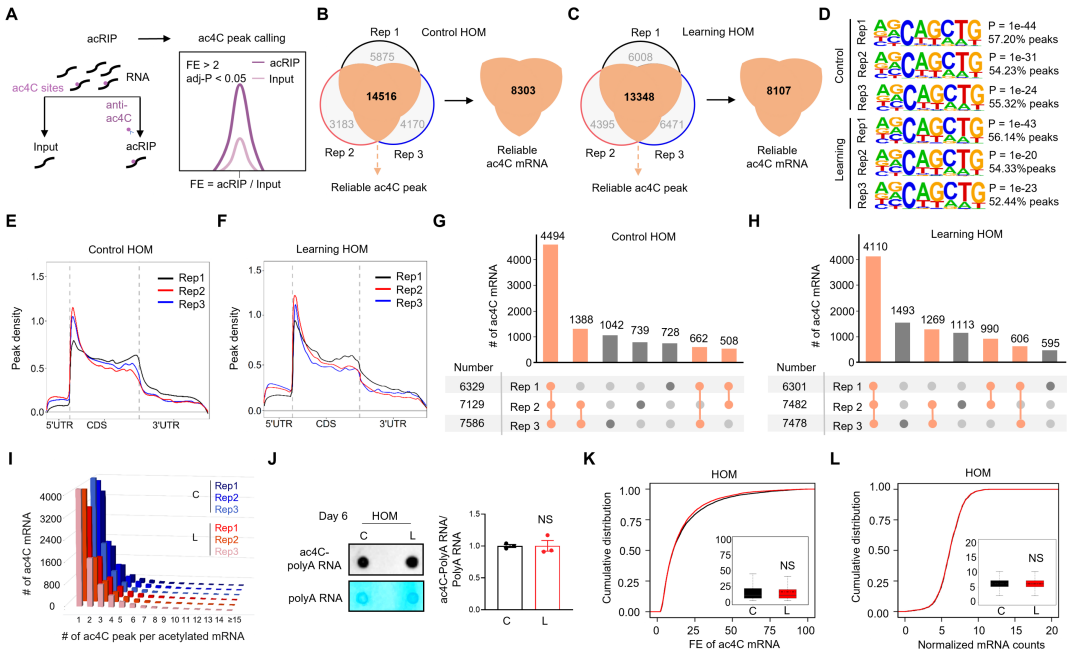

Supplementary Figure 2 No significant change of ac4C mRNA in the homogenates of mouse hippocampus after memory. (A) Experimental design. The RNA samples were divided into input and acRIP. Among them, input was used to eliminate background and acRIP was performed with ac4C antibodies. The process of sequencing peak calling identifies reliable ac4C peaks and calculates FE for each ac4C peak based on the sequencing information of the two-part sample. FE, Fold Enrichment. (B and C) Venn diagrams demonstrating substantial overlap of ac4C peaks and ac4C-modified mRNAs across biological replicates in control mice. (B) Venn diagram showing the intersection of ac4C peaks among three biological replicates from hippocampal homogenates (HOM) of control mice on day 6. The numbers indicate unique and shared peaks between replicates, with 8303 peaks common to all three replicates. (C) Venn diagram showing the intersection of ac4C-modified mRNAs among the same three biological replicates, with 8107 mRNAs common to all three replicates. (D) Consensus motif analysis reveals consistent ac4C modification patterns across biological replicates in both control and learning groups. HOMER motif analysis identified the identical consensus sequence AGCAGCTG in ac4C peak regions across all biological replicates. For control mice, the motif shows highly significant p-values with target percentages at 99% confidence intervals of 57.20% (Rep 1), 54.23% (Rep 2), and 55.32% (Rep 3). For learning mice, similarly significant p-values were observed with target percentages of 56.14 (Rep 1), 54.32% (Rep 2), and 52.44% (Rep 3). The consistency of this motif across both conditions and all replicates demonstrates the specificity of ac4C modification sites. (E and F) Distribution of ac4C peak density along mRNA transcripts in control and learning groups. Metagene profiles display the relative density of ac4C peak coverage across different regions of acetylated mRNAs. Peak density distribution in HOM samples shows enrichment primarily within the CDS region, with lower density in the 5' and 3' UTRs. The analysis encompasses all three biological replicates from control (E) and learning groups (F). (G-H) Upset plots illustrating the overlap patterns of ac4C peaks across biological replicates. (G) Upset plot displaying the intersection of ac4C peaks among three biological replicates from control HOM

samples. The analysis reveals 4494 peaks common to all three replicates, with varying numbers of peaks shared between pairs of replicates or unique to individual samples. (H) Upset plot showing the intersection of ac4C peaks among three biological replicates from learning HOM samples. The analysis identifies 4110 peaks common to all three replicates. The distribution patterns and overlap characteristics remain comparable between control and learning conditions, further supporting the stability of ac4C modifications after memory formation. (I) The number of ac4C peaks for each ac4C mRNA is comparable across the three biological replicates in both the HOM control and learning groups. (J) Acetylation of polyA RNA was not altered in HOM of mouse hippocampus after memory. The polyA RNA samples used for each ac4C dot-blot were 0.5 mg that falls into the linear range. The HOM polyA RNA samples of control and learning mice on day 6 after MWM training were subjected to ac4C dot-blots and methylene blue staining. Left, representative images of ac4C dot-blots and methylene blue staining; right, quantification data. n = 3 biological replicates at each condition, NS, not significant, two-tailed t-test. Data were normalized by controls. (K) Acetylation levels of ac4C mRNA were not significantly changed after memory in HOM of mouse hippocampus. Shown are cumulative distribution curves of ac4C levels for HOM in control (C) and learning (L) mice on day 6 after MWM training. The FE of ac4C mRNA was quantified in the quartile boxplots, where the solid line in the box is the median and the dashed line is the mean, where the maximum and minimum values are identified. NS, not significant, Kolmogorov-Smirnov test. FE, Fold Enrichment. (L) The normalized mRNA counts were not significantly changed in HOM of mouse hippocampus on day 6 after MWM training. Shown are cumulative distribution curves of normalized mRNA counts for HOM in C and L mice on day 6 after MWM training. The normalized mRNA counts of each group were quantified in the quartile boxplots, where the solid line in the box is the median and the dashed line is the mean, where the maximum and minimum values are identified. NS, not significant, Kolmogorov-Smirnov test.

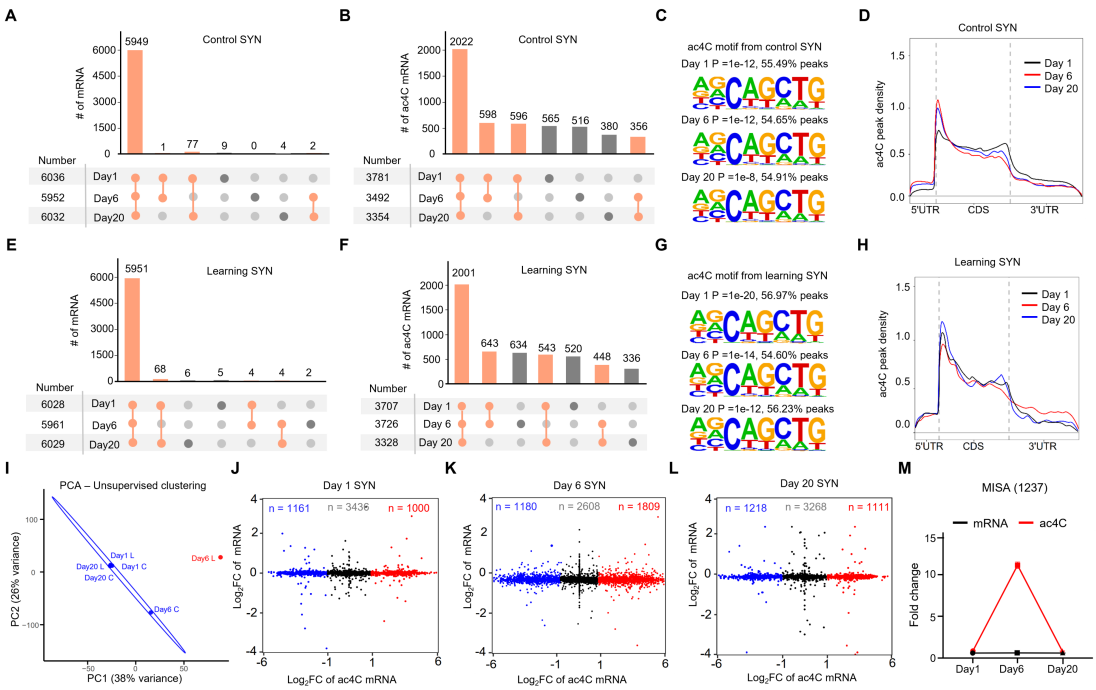

Supplementary Figure 3 Memory-induced synaptic ac4C mRNAs (MISA) in mouse hippocampus. (A-B and E-F) The transcripts and ac4C mRNAs are largely overlapping across the SYN control group (A-B) and learning group (E-F) at days 1, 6, and 20. The upset plot shows the number of mRNAs (A and E) and ac4C mRNAs (B and F) between samples. (C and G) The same consensus motif, AGCAGCTG, was identified in ac4C peak regions across the SYN control (C) and learning group (G) at days 1, 6, and 20. Consensus motif and its adjusted p-values generated by HOMER of the SYN group at days 1, 6, and 20 in acRIP-seq. (D and H) Density of ac4C peaks across different mRNA regions in the SYN control group (D) and SYN learning group (H) at days 1, 6, and 20. The line plot illustrates the density distribution of ac4C peaks in 5'UTR, CDS, and 3'UTR. The black line represents day 1, the red line represents day 6, and the blue line represents day 20. (I) PCA to demonstrate that the sample SYN learning-day6 separates from the other five samples. (J-L) Scatter plot showing the correlation between changes in mRNA expression and acetylation levels on days 1, 6, and 20. The x-axis represents the fold change in acetylation levels, while the y-axis shows the fold change in mRNA expression. (M) The ac4C levels of MISA mRNA are upregulated following memory and return to control levels after memory retrieval. At days 1, 6, and 20, there are no significant changes in MISA mRNA levels. The black

line represents the trend of mRNA expression changes, and the red line represents the trend of ac4C level changes.

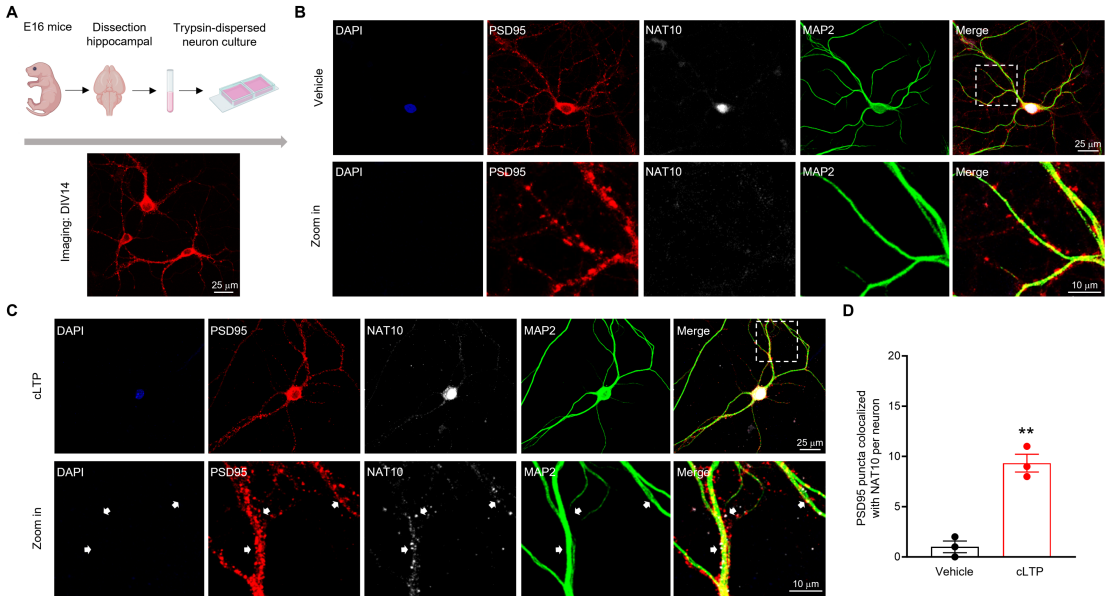

Supplementary Figure 4 Increase of NAT10 proteins in the SYN of cultured hippocampal neurons after cLTP stimulation. (A) Experimental design. (B and C) Distribution of NAT10 in the PSD were increased in cultured hippocampal neurons after chemical LTP stimulation. Shown are the fluorescent images of NAT10 were significantly increased in the PSD fraction of primary neuronal of mouse hippocampal after cLTP stimulated. Scale bar, 25 μm and 10 μm. (D) Quantification of PSD95 puncta colocalized with NAT10 per neuron. ** P = 0.0014, two-tailed t-test. Data represent results from three independent experiments.

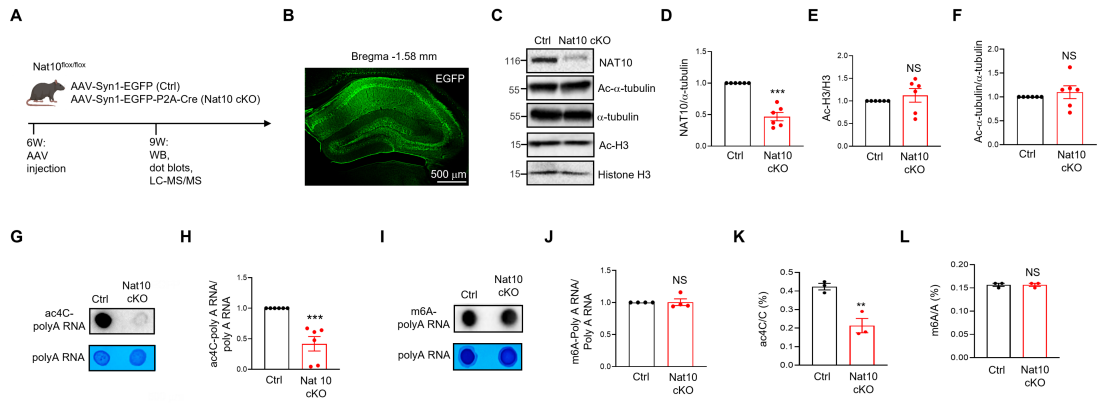

Supplementary Figure 5 NAT10-dependent ac4C modification of polyA RNA in

1770 **mouse hippocampus.** (A) Experimental design. Three weeks after AAV injection, Ctrl
1771 and Nat10 cKO mice underwent MWM training and probe test, followed by
1772 hippocampal tissue collection for biochemical assays. (B) Infection of AAV in the
1773 dorsal mouse hippocampus. Fluorescent images of the mouse hippocampus expressing
1774 EGFP are shown. Scale bar, 500 μm. (C) Representative western blot images. Protein
1775 samples from Ctrl and Nat10 cKO mouse hippocampus were probed with antibodies
1776 against NAT10, Ac-α-tubulin, α-tubulin, Ac-H3, and Histone H3. (D) Reduction of
1777 NAT10 protein levels in Nat10 cKO mice compared to Ctrl. Quantification data for
1778 panel **C** are shown. *** $P < 0.001$, two-tailed t-test, n = 6 biological replicates per
1779 condition, Data were normalized by controls. (E) Similar ac-H3 levels between Ctrl and
1780 Nat10 cKO mice. Quantification data for panel **C** are shown. NS, not significant, two-
1781 tailed t-test, n = 6 biological replicates per condition, Data were normalized by controls.
1782 (F) Similar Ac-α-tubulin levels in Ctrl and Nat10 cKO mice. Quantification data for
1783 panel (C) are shown. NS, not significant, two-tailed t-test, n = 6 biological replicates
1784 per condition, Data were normalized by controls. (G and H) Reduced ac4C modification
1785 of polyA RNA in the hippocampus of Nat10 cKO mice, compared with controls. The
1786 polyA RNA samples purified from the HOM of mouse hippocampus were subjected to
1787 ac4C dot-blots and methylene blue staining. (G) Representative images. (H)
1788 Quantification data. *** $P < 0.001$, two-tailed t-test, n = 6 biological replicates per
1789 condition. Data were normalized by controls. (I and J) Similar m6A modification of
1790 polyA RNA in the hippocampus of control and Nat10 cKO mice. The polyA RNA
1791 samples purified from the HOM of mouse hippocampus were subjected to m6A dot-
1792 blots and methylene blue staining. (I) Representative images. (J) Quantification data.
1793 NS, not significant, two-tailed t-test, n = 4 biological replicates per condition. (K)
1794 Reduced ac4C modification of polyA RNA in the hippocampus of Nat10 cKO mice,
1795 compared with controls. The polyA RNA samples purified from the HOM of mouse
1796 hippocampus were subjected to LC-MS/MS analysis. The stoichiometry levels of ac4C
1797 from LC-MS/MS analysis were quantified. ** $P = 0.0077$, two-tailed t-test, n = 3
1798 biological replicates per condition. (L) Similar m6A modification of polyA RNA in the

hippocampus of control and Nat10 cKO mice. The polyA RNA samples purified from the HOM of mouse hippocampus were subjected to LC-MS/MS analysis. The stoichiometry levels of m6A from LC-MS/MS analysis were quantified. NS, not significant, two-tailed t-test, n = 3 biological replicates per condition.

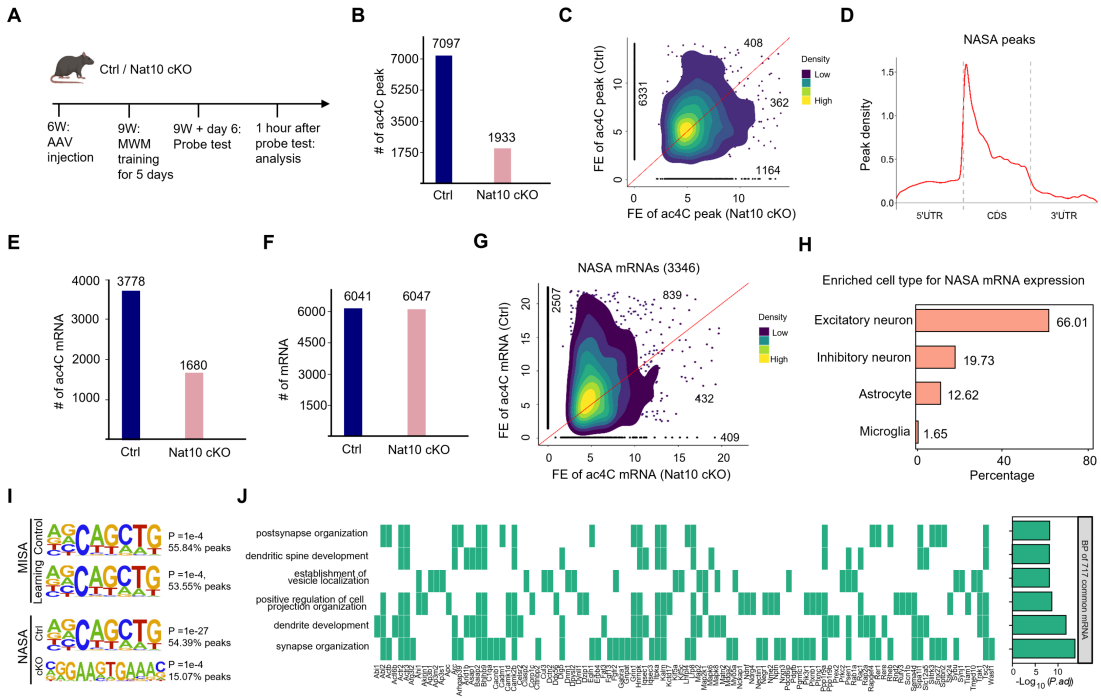

Supplementary Figure 6 NAT10-dependent of ac4C mapping in the SYN of memory mice. (A) Experimental design. Three weeks after AAV injection, the control (Ctrl) and Nat10 conditional knockout (cKO) mice were subjected to MWM training and probe test, and then the SYN fractions were purified from hippocampal tissues for low-input acRIP-seq. (B) Reduction of ac4C peak number in the SYN of Nat10 cKO mice, compared with controls. 7097 and 1933 ac4C peaks were identified in the SYN of control and Nat10 cKO mice, respectively. (C) Definition of NAT10-dependent ac4C peaks through acRIP summits displaying higher FE values in control relative to Nat10 cKO mice. Shown are the density scatter plot of ac4C peaks. Each dot represents an ac4C peak. 6331 ac4C peaks are specifically identified in the SYN of control but not Nat10 cKO mice. The FE of 408 ac4C peaks was higher in the SYN of control mice than Nat10 cKO mice. (D) NAT10-dependent ac4C peaks are predominantly located in

the CDS region of mRNA. The plot shows the density of ac4C peaks along various mRNA regions, including the 5'UTR, CDS, and 3'UTR. (E) Reduction of ac4C mRNA number in the SYN of Nat10 cKO mice, compared with controls. 3778 and 1680 ac4C mRNAs were identified in the SYN of control and Nat10 cKO groups, respectively. (F) Similar mRNA numbers identified in the SYN of control and Nat10 cKO mice. 6041 and 6047 mRNAs were identified in the SYN of control and Nat10 cKO mice, respectively. (G) Definition of NAT10-dependent synaptic ac4C (NASA) mRNA through acRIP summits displaying higher FE values in control relative to Nat10 cKO mice. Shown are the density scatter plot of ac4C mRNA. Each dot represents an ac4C mRNA. 2507 ac4C mRNAs are specifically identified in the SYN of control but not Nat10 cKO mice. The FE of 839 ac4C mRNA was higher in the SYN of control mice than Nat10 cKO mice. (H) The expression of NASA mRNA is mostly enriched in excitatory neurons of mouse hippocampus. Shown are the percentage of NASA mRNA whose expression was relatively enriched in different cell types of mouse hippocampus through analysis of the single-cell RNA-sequencing dataset (http://dropviz.org). (I) A shared consensus motif, AGCAGCTG, was consistently enriched within ac4C peak regions in both the MISA and NASA groups, as identified by HOMER from acRIP-seq data. Notably, in Nat10 cKO samples, the ac4C-associated motifs exhibited a marked loss of the CXX sequence feature, suggesting that Nat10 depletion alters the sequence preference for ac4C deposition. (J) Gene Ontology BPs associated with the 717 common mRNAs from Figure 6D are significantly enriched. The x-axis indicates both the included mRNAs and the negative logarithm of the adjusted p-values, representing enrichment significance, while the y-axis displays the corresponding biological processes.

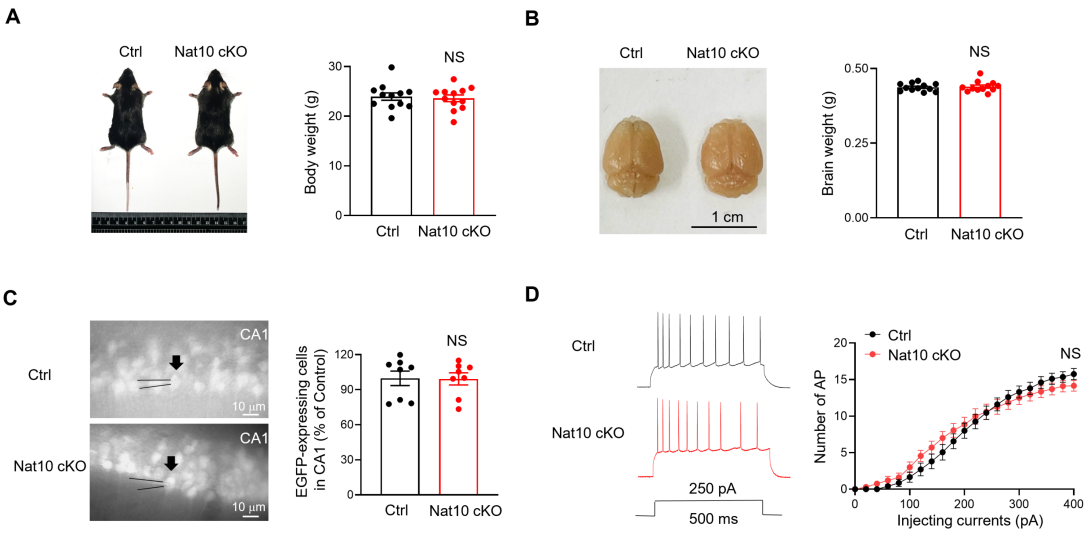

Supplementary Figure 7 Downregulation of NAT10 in mouse hippocampus does not affect body or brain weight, neuronal number or intrinsic excitability. (A) Similar body weight between 10-week-old Ctrl and Nat10 cKO mice. Left, representative images of the mice, right, quantification of body weight. n = 12 mice for each group, NS, not significant, two-tailed t-test. (B) Similar brain weight between 10-week-old Ctrl and Nat10 cKO mice. Left, representative images of mouse brain, right, quantification of brain weight. n = 12 mice for each group, NS, not significant, two-tailed t-test. (C) Similar number of neurons expressing EGFP in the CA1 region of 10-week-old Ctrl and Nat10 cKO mice. Left, representative images of CA1 neurons expressing EGFP, right, quantification of EGFP-expressing cells in CA1 region. n = 8 slices from 4 mice, NS, not significant, two-tailed t-test. Data were normalized by Ctrl. (D) Similar intrinsic excitability of CA1 pyramidal neurons between 10-week-old Ctrl and Nat10 cKO mice. Left, representative traces of action potentials (AP) of CA1 pyramidal neurons; right, quantification of AP number after injection of different currents into CA1 pyramidal neurons. n = 20 cells from 4 mice per group, NS, not significant, two-way ANOVA followed by Sidak's multiple comparison test.

Supplementary Tables

Supplementary Table 1. Library Information of acRIP-seq.

Supplementary Table 2. List of mRNAs identified by regular acRIP-seq (HOM).

Supplementary Table 3. List of mRNAs identified by low-input acRIP-seq (SYN).

1864 Supplementary Table 4. The information of MISA mRNA.

1865 Supplementary Table 5. The information of NASA mRNA.